AJAE

Open Access

Vol. 14, No. 3, pp. 177-209, September 2020
doi: https://doi.org/10.5572/ajae.2020.14.3.177
ISSN (Online) 2287-1160, ISSN (Print) 1976-6912

Review Article

Aerosol Hygroscopicity on A Single Particle Level Using Microscopic and Spectroscopic Techniques: A Review

Li Wu, Chul-Un Ro*

Department of Chemistry, Inha University, Incheon 22212, Republic of Korea

***Corresponding author.**
Tel: +82-32-860-7676
E-mail: curo@inha.ac.kr

Received: 15 July 2020
Revised: 1 September 2020
Accepted: 7 September 2020

ABSTRACT Studies on the hygroscopic properties of aerosol particles can provide critical insights into important aerosol properties such as (1) alteration of aerodynamic properties; (2) cloud-droplet nucleation efficiency; (3) optical properties; and (4) physicochemical changes through complex heterogeneous chemical reactions with atmospheric gas-phase species. Investigations of the hygroscopic properties have been carried out using various analytical techniques for individual or bulk aerosol particles with deviating chemical compositions. Solid information on the hygroscopic properties, morphology, and chemical composition of airborne particles on a micrometer scale can be achieved by using a single particle approach. In this short review, recent microscopic (such as optical microscope, atomic force microscopy, environmental SEM and TEM, and scanning transmission X-ray microscopy) and spectroscopic (including Raman microspectrometry, FTIR spectroscopy, and their combination with levitation techniques) studies of hygroscopicity of aerosol particles on a single particle level are provided.

KEY WORDS Hygroscopicity, Single particle analysis, Microscopic and spectroscopic techniques

1. INTRODUCTION

Atmospheric aerosol particles composed of inorganic and organic species in various phase states play significant roles in global climate change directly by scattering or absorbing incoming solar radiation and indirectly by serving as cloud condensation nuclei (CCN) and/or ice nuclei (IN) (Seinfeld and Pandis, 2016). The radiative effects, optical properties, and chemical reactivity of atmospheric aerosol particles depend on their chemical compositions, sizes, aerosol phases, and mixing states (Martin, 2000). Studies on the heterogeneous chemistry of aerosol particles in the air is of vital importance, since airborne particles can react with gaseous pollutants, such as SO_x or NO_x, and their physicochemical properties can be modified in turn, through heterogeneous chemical reactions. In addition, the chemistry of the Earth's atmosphere is influenced by reducing photolysis rates of important atmospheric gas-phase species through heterogeneous chemical reactions with the atmospheric aerosol particles. Therefore, increasing attention has been devoted to the study of

physicochemical characteristic changes of aerosol particles (Poschl and Shiraiwa, 2015; Usher *et al.*, 2003). It has been well recognized that the ability of aerosol particles to contain water as a function of relative humidity (RH), referred to as the hygroscopicity, plays important roles in some heterogeneous reactions (Freedman, 2017; Tang *et al.*, 2016a, b). For example, gaseous HNO_3 can be dissolved in the surface water and gradually react with $CaCO_3$ particles which originally do not absorb a significant amount of water on the surface, resulting in the total consumption of $CaCO_3$ species, the completion of irreversible heterogeneous reaction, and the production of hygroscopic $Ca(NO_3)_2$ species (Kelly, 2005). When the chemical compositions of particles are modified by aging processes including heterogeneous reactions, their hygroscopic properties are altered accordingly, which in turn alters their phase states. Thus, $Ca(NO_3)_2$ particles were observed as liquid droplets when they were formed in the air (Laskin *et al.*, 2005; Krueger *et al.*, 2004; Krueger, 2003). Furthermore, hygroscopicity of particles determines their size and refractive index, affecting their optical properties and consequently their impacts on visibility and direct radiative forcing (Tang *et al.*, 2019; Krieger *et al.*, 2012).

Since the understanding of the hygroscopic properties of airborne particles is important to analyze their physicochemical changes (Krieger *et al.*, 2012), there have been many studies on the deliquescence and efflorescence behaviors of atmospheric-related aerosol particles (Freney *et al.*, 2009; Mikhailov *et al.*, 2009; Wise *et al.*, 2007; Hoffman *et al.*, 2004; Ebert *et al.*, 2002; Martin, 2000; Ge *et al.*, 1998, 1996; Tang and Fung, 1997; Tang and Munkelwitz, 1994; Cohen *et al.*, 1987a, b, c). The sizes of hygroscopic particles in the atmosphere can vary depending on the ambient RH. In other words, particles can grow by absorbing water with increasing RH (humidification process) or shrink when water evaporates with decreasing RH (dehydration process). For aerosol particles which can deliquesce and effloresce during humidification and dehydration processes, respectively, the size of dry particles remains unchanged with increasing RH until the deliquescence RH (DRH) is reached, after which the solid particles become aqueous droplets, and they experience hygroscopic growth above the DRH. When RH is decreased, the concentration of salts in the aqueous droplets becomes dense and can finally crystallize at their efflorescence RH (ERH).

For atmospheric aerosol particles, deliquescence is a thermodynamic process and a range of thermodynamic models, such as the Extended Atmospheric Inorganics Model (E-AIM) (http://www.aim.env.uea.ac.uk/aim/aim.php) and the Aerosol Inorganic-Organic Mixtures Functional groups Activity Coefficient (AIOMFAC) model (http://www.aiomfac.caltech.edu), have been developed to predict the deliquescence behavior or the ionic activity coefficients of single or two-component aerosol particles (Zuend *et al.*, 2012, 2011; Wexler and Clegg, 2002; Ansari and Pandis, 1999; Clegg *et al.*, 1998; Tang, 1976). Efflorescence is a kinetic or rate-driven process that occurs by overcoming a kinetic barrier, which in turn depends on a range of factors, such as the solubility and concentration of the chemical components, vapor pressure, interfacial tension, inter-ionic forces, solute-water and solute-solute interactions, etc. (Martin, 2000). Therefore, the best way to understand efflorescence behavior of aerosol particles is through experimental measurements (Seinfeld and Pandis, 2016). It is also known that the ERH of aerosols is sometimes significantly lower than their DRH, which is called hysteresis.

Regarding the deliquescence of a two-component inorganic solid mixture, it has been predicted theoretically that two-stage phase transitions should occur, i.e. an aqueous phase with a eutonic composition is formed first at their mutual DRH (MDRH), and the remnant solids in the core dissolve later at their second DRH which depends on the composition of the particle (Wexler and Seinfeld, 1991). The MDRH should be independent of the mixing ratios of the two-component salt mixtures and the MDRH in multi-component systems should always be lower than the DRHs of the pure individual salts (Wexler and Seinfeld, 1991). Multi-component aqueous droplets should show step-wise efflorescence transitions: a component in the aqueous droplets precipitates first at their ERH and the aqueous phase of the eutonic composition effloresces at their mutual ERH (MERH), therefore, forming a heterogeneous, core-shell crystal structure (Ge *et al.*, 1996). Full phase diagrams, covering the entire range of mixing ratios, are generally helpful to fully understand the hygroscopic behavior of multi-component aerosol particles (Martin, 2000).

Numerous studies on the hygroscopic properties of particles with various chemical compositions have been carried out using diverse analytical techniques (Tang *et al.*, 2019; Krieger *et al.*, 2012). The particles can be either collected by a cascade impactor aerosol sampler or generated through an atomizer from aqueous solutions. All the

analytical techniques have proved to be very useful for studies on the hygroscopic properties of different types of particles under controlled RH. For example, rapid single particle mass spectrometry (Ge *et al.*, 1998, 1996) and online Fourier transform infrared (FTIR) spectroscopy (Braban *et al.*, 2001; Cziczo and Abbatt, 2000; Cziczo *et al.*, 1997) were used to examine the hygroscopic properties of aerosol particles, depending on their chemical compositions or mixing states. Hygroscopicity-tandem differential mobility analyzer (H-TDMA) has been widely used for the hygroscopic studies of size-segregated mono-disperse aerosol particles (typically in sub-micrometer range) (Mikhailov *et al.*, 2009; Gysel *et al.*, 2002; Weingartner *et al.*, 2002; Rader and McMurry, 1986). Because H-TDMA cannot provide chemical compositional information on aerosol particles, the H-TDMA system has sometimes been combined with other techniques, such as scanning or transmission electron microscopy (SEM/TEM), single-particle laser-ablation time-of-flight mass spectrometry (SPLAT-MS), or aerosol time-of-flight mass spectrometry (ATOFMS) (Park *et al.*, 2009; Herich *et al.*, 2009, 2008; Zelenyuk *et al.*, 2008; McMurry *et al.*, 1996). In addition, the hygroscopic properties of single particles can be examined using levitation techniques (Krieger *et al.*, 2012; Lee *et al.*, 2008; Tang *et al.*, 2007; Parsons *et al.*, 2006; Tang *et al.*, 1997; Tang and Fung, 1997; Tang and Munkelwitz, 1994; Cohen *et al.*, 1987a, b, c). To obtain the chemical compositions along with the hygroscopic properties of single particles, the levitation techniques have been used in combination with nonintrusive analytical techniques such as electro-dynamic balance (EDB) with Raman microspectrometry (RMS), laser induced fluorescence, or Mie-scattering (Treuel *et al.*, 2010; Lee *et al.*, 2008; Choi and Chan, 2005; Choi *et al.*, 2004; Tang and Fung, 1997) and optical levitation with RMS (Jordanov and Zellner, 2006). On the other hand, many hygroscopic studies have been performed for individual or bulk aerosol particles collected on a range of substrates such as TEM grids, silicon wafer. ZnSe window, and Si_3N_4 window by micro-FTIR in a flow-cell or static mode chamber (SMC) (Ghorai *et al.*, 2011; Liu *et al.*, 2008a; Lu *et al.*, 2008; Braban *et al.*, 2001). The hygroscopicity of submicrometer salt particles were studied by scanning transmission X-ray microscopy/X-ray absorption spectroscopy (STXM/XAS) and noncontact environmental atomic force microscopy (e-AFM), using a Si_3N_4 X-ray transmission window (Ghorai *et al.*, 2011; Zelenay *et al.*, 2011) and oxidized silane-treated silicon wafer (Bruzewicz *et al.*, 2011) as the substrate, respectively. The liquid water content of aerosol particles deposited on Fluoropore and Teflon filters was determined by gravimetric analysis and ion chromatography (McInnes *et al.*, 1996) and by gas chromatography with a thermal conductivity detector (Lee and Chang, 2002; Lee and Hsu, 2000; Hsu, 1998), respectively. Some excellent review papers focusing on the techniques for investigating aerosol hygroscopicity of aerosol particles have been published in the previous studies (Tang *et al.*, 2019, 2016a; Kreidenweis and Asa-Awuku, 2014; Krieger *et al.*, 2012; Swietlicki *et al.*, 2008). Latest advances for characterizing complex chemical and physical properties of atmospheric aerosols using key spectroscopic and microscopic techniques were also summarized and discussed (Ault and Axson, 2017). For further details, interested readers are directed to those literatures.

Atmospheric particles are chemically and morphologically heterogeneous so that the average composition and aerodynamic diameter, which are closely related to their physicochemical properties, obtained from bulk analyses do not describe well the chemical modification of the particles. Nevertheless, single particle analysis can provide the hygroscopic properties, morphology, chemical composition, mixing state, and heterogeneous reactions of airborne particles on a micrometer scale (Li *et al.*, 2016; Ro *et al.*, 2005). In addition, microscopic and spectroscopic techniques could simultaneously investigate the hygroscopic growth, phase transformation, chemical compositional evolution, and morphological changes of individual aerosol particles according to relative humidity change (Gupta *et al.*, 2015a).

In this review, hygroscopic studies on a single particle level using microscopic and spectroscopic techniques will be provided in two major sections. The microscopic section includes hygroscopic system coupled with optical microscope, atomic force microscopy, environmental SEM and TEM, and scanning transmission X-ray microscopy. The spectroscopic section covers in-situ Raman and FTIR and the levitation techniques. For each technique, some typical results are introduced for better elucidating how these techniques contribute to investigation of hygroscopicity of aerosol particles.

2. MICROSCOPIC STUDIES

Hygroscopicity on a single-particle level can be stud-

ied using various microscopic techniques. Visual observation on changes in particle size at different RHs can be used to determine hygroscopic growth factors and phase transitions (Tang *et al.*, 2019).

2. 1 Optical Microscopy (OM)

Optical microscopy (OM) with an apparatus which produces an air stream of variable humidity was first utilized to perform humidification measurement of single aerosol particles collected in Sydney, which were sea-salts based on their solid-to-liquid phase transition occurring in the range of ~71–75% (Twomey, 1954, 1953).

A flow cell coupled with OM was employed to study the deliquescence behavior of malonic, succinic, glutaric, and adipic acid particles of 2–40 μm size, for which the results were in agreement with those from the literature and model calculations (Parsons *et al.*, 2004b). The similar apparatus was then employed to investigate the hygroscopic behavior of ammonium sulfate (AS) and NaCl mixed with glutaric acid particles and AS particles mixed with water-soluble organic compounds, showing that the organic compounds only slightly influence the DRHs of the inorganic moiety, while they may drastically decrease the ERHs of the inorganic components depending on their types and concentrations (Pant *et al.*, 2004; Parsons *et al.*, 2004a). Soot and kaolinite particles were reported to have no impact on the ERH of the AS droplets and to increase it, respectively, using the above apparatus (Pant *et al.*, 2006).

An OM technique was used to perform the visual observation of the phase transformation and hygroscopic growth of aerosol particles on a single particle level (Ahn *et al.*, 2010). Fig. 1 shows the schematic diagram of the setup, which is composed of three parts: (A) the see-through impactor, (B) an optical microscope, and (C) a humidity controlling system (Ahn *et al.*, 2010). Collecting substrates, such as TEM grids, Al, and Ag foils on which either wet or dry deposited particles were seated, were placed on the impaction plate in the see-through impactor. The RH inside the impactor was controlled by mixing dry and wet (saturated with water vapor) N_2 gases. The wet N_2 gas was obtained by bubbling through deionized water reservoirs. The flow rates of the dry and wet N_2 gases were controlled by mass flow controllers (MFC) to obtain the desired RH in the range of ~3–95%, which was monitored using a digital hygrometer (Testo 645). Optical images that contained information on the phase transformation and hygroscopic growth of individual particles according to RH change were recorded by using a digital camera through an optical microscope as shown in Fig. 2 (Eom *et al.*, 2014). The change in size of the individual particles on optical images was used to generate growth factors (GFs) by dividing two-dimensional (2-D) areas of the particle at different RHs by that of the dry particle before starting the humidification process. From the 2-D area measurement of all the particles in the image field at each RH, the humidification and dehydration curves for all the particles were obtained as shown in Fig. 3, so that DRHs and ERHs of the particles can be determined (Ahn *et al.*, 2010). Particles larger

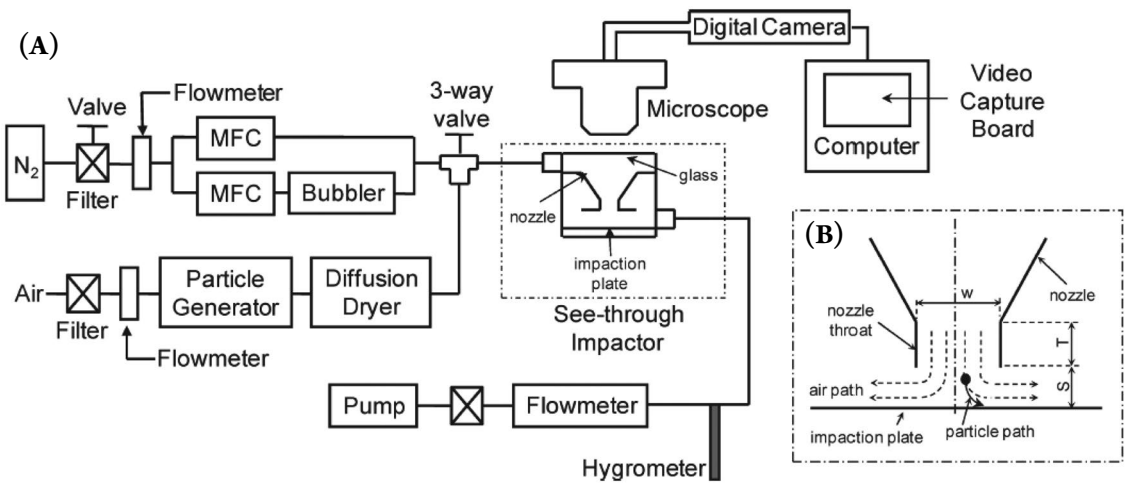

Fig. 1. Schematic diagram of the measurement setup for hygroscopic properties of individual particles. Reprinted with permission from Ahn, K.-H., Kim, S.-M., Jung, H.-J., Lee, M.-J., Eom, H.-J., Maskey, S., Ro, C.-U., Anal. Chem. 2010, 82, 7999–8009. Copyright 2010 American Chemical Society.

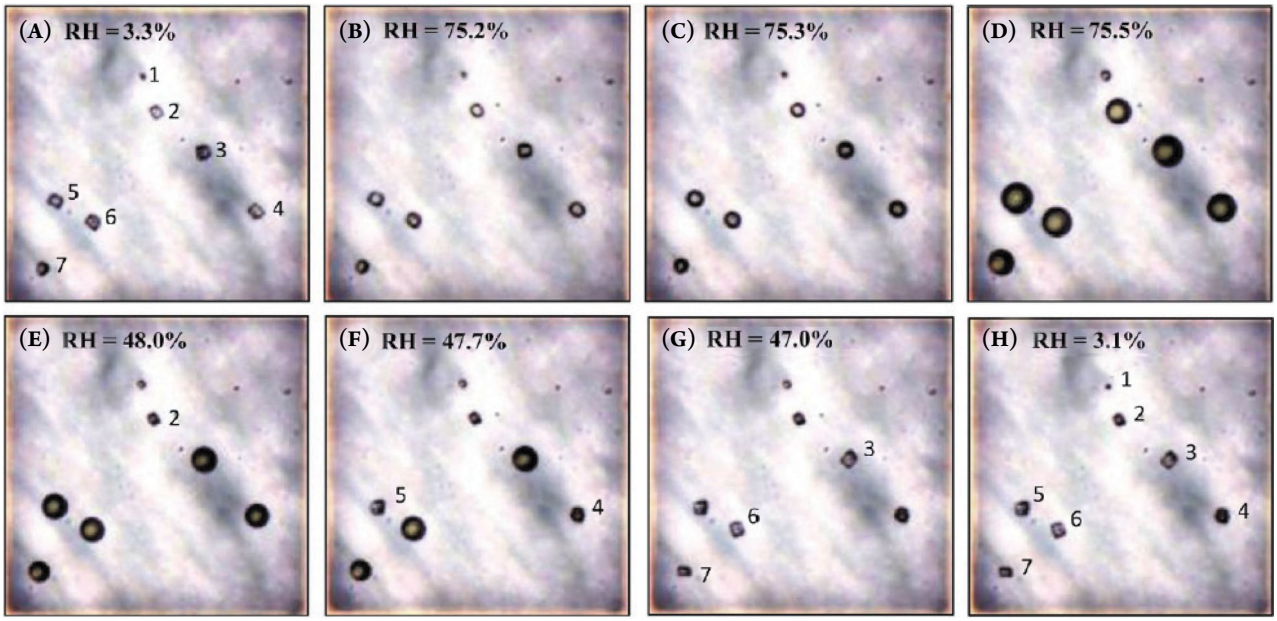

Fig. 2. Optical images obtained during the (A–D) humidification process and (E–H) dehydration process for generated NaCl particles on the TEM grid. Reprinted with permission from Eom, H.J., Gupta, D., Li, X., Jung, H.J., Kim, H., Ro, C.U., Anal. Chem. 2014, 86, 2648–2656. Copyright 2014 American Chemical Society.

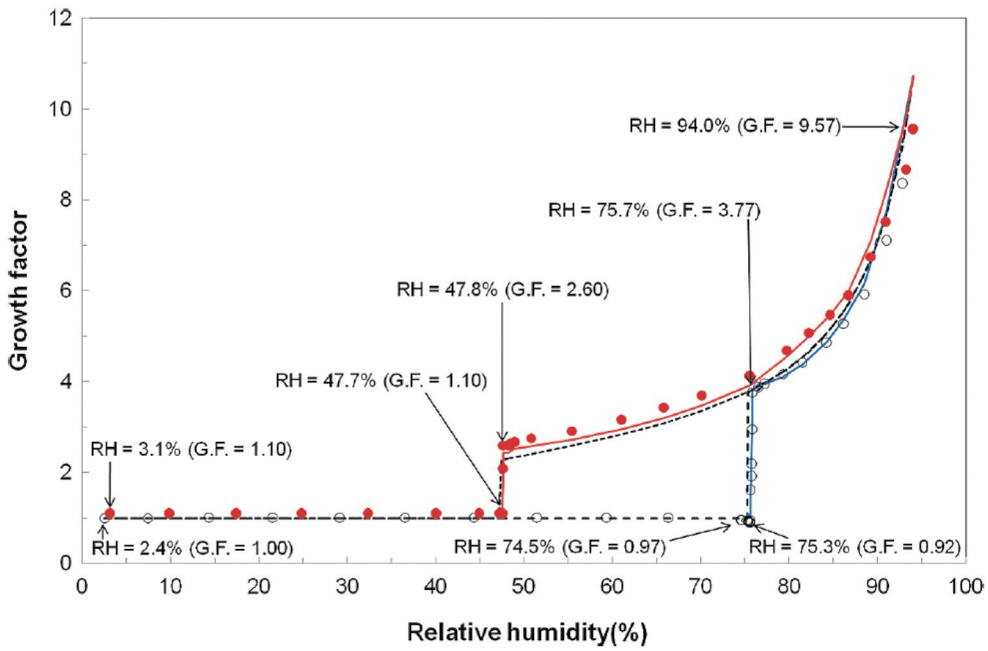

Fig. 3. Humidification and dehydration curves for a typical NaCl particle collected on a TEM grid. Blank and solid circles are growth factor (GF) data obtained during the humidification and dehydration processes, respectively. The growth factors were obtained by dividing areas of the particle at different RHs by that of the dry particle before starting the humidification process. Humidification and dehydration curves, represented as growth factors in mass, are plotted in solid lines. Humidification and dehydration curves from Tang *et al.*, 1997 are also shown in dotted lines for comparison. Reprinted with permission from Ahn, K.-H., Kim, S.-M., Jung, H.-J., Lee, M.-J., Eom, H.-J., Maskey, S., Ro, C.-U., Anal. Chem. 2010, 82, 7999–8009. Copyright 2010 American Chemical Society.

than ~0.5 μm could be analyzed using this system. The practical applicability of this analytical methodology was validated by investigating the hygroscopic properties of artificially generated NaCl, KCl, $(NH_4)_2SO_4$, and Na_2SO_4 aerosol particles of micrometer size collected on TEM grid, which were well agreed with those reported in the literature. The technique was then employed to characterize the hygroscopic properties on individual ambient aerosol particles containing two or three components and energy-dispersive electron probe X-ray microanalysis (ED-EPMA) was used to perform a quantitative chemical speciation of the same individual particles after the measurement of the hygroscopic property (Ahn *et al.*, 2010), which clearly identified the hygroscopic properties and morphologies of pure, reacted, and mixed sea-salt, mineral, and carbonaceous particles.

Hygroscopic studies using the analytical system on a single-particle basis were performed for laboratory-generated single or mixed inorganic particles. The hygroscopic behavior of wet dispersed and dry deposited $NaNO_3$ particles of 2.5–4 μm was examined (Kim *et al.*, 2012). Most of wet dispersed $NaNO_3$ particles continuously grew and shrank during humidification and dehydration processes, respectively, and yet all the dry deposited particles had reproducible DRHs and ERHs. The different behavior of the $NaNO_3$ particles is attributed to different nucleation mechanisms, i.e. the homogeneous and heterogeneous nucleations, for pure and impure (seed-containing) $NaNO_3$ particles, respectively (Kim *et al.*, 2012). Similar observation was reported for ammonium nitrate (AN) (Sun *et al.*, 2018; Cziczo and Abbatt, 2000; Lee and Hsu, 2000; Lightstone *et al.*, 2000; Dougle *et al.*, 1998; Neubauer *et al.*, 1998; Tang, 1980) and NH_4HSO_4 (Cziczo and Abbatt, 2000; Lee and Hsu, 2000; Tang and Munkelwitz, 1994; Mozurkewich and Calvert, 1988).

A study systematically examined full hygroscopic properties of NaCl and KCl mixture aerosol particles in nine mixing ratios (mole fractions of KCl (X_{KCl}) = 0.1–0.9), obtained experimental phase diagrams for their deliquescence and efflorescence, and elucidated the efflorescence mechanism (Li *et al.*, 2014c). K and Na salts are major components of sea salt (Seinfeld and Pandis, 2016) and KCl is also a major constituent of young smoke produced from biomass burning along with soot particles (Pósfai *et al.*, 2003). Stepwise deliquescence and single-stage efflorescence transitions were observed. Elemental X-ray mappings of the effloresced NaCl-KCl mixture particles at all mixing ratios were performed using SEM/EDX for better understanding the efflorescence process and it was suggested that a more supersaturated salt homogeneously nucleated to be crystallized in the center and the other salt almost simultaneously underwent the heterogeneous crystallization on the former (Li *et al.*, 2014c).

The influence of six collecting substrates with different physical properties (see Table 1) on the hygroscopicity measurements of inorganic aerosol surrogates and the potential applications of these substrates by optical microscopy were examined (Eom *et al.*, 2014). The TEM grids were found to be most suitable for the hygroscopic measurements of individual inorganic aerosol particles by optical microscopy, especially when multiple analytical

Table 1. General characteristics of six different substrate materials used for hygroscopic measurements. Reprinted with permission from Eom, H.J., Gupta, D., Li, X., Jung, H.J., Kim, H., Ro, C.U., Anal. Chem. 2014, 86, 2648–2656. Copyright 2014 American Chemical Society.

Substrate property	TEM grid	Parafilm-M	Aluminum (Al) foil	Silver (Ag) foil	Silicon wafer	Cover glass
Supplier	Ted Pella Inc., USA	Pechiney Plastic Packaging Company, USA	Goodfellow Inc., UK	Goodfellow Inc., UK	MTI Corp., USA	Menzel-Gläser, Germany
Purity (%)	99.99	–	99.0	99.95	99.999	–
Thickness (mm)		0.127	0.025	0.025	0.27	0.13–0.16
Physical resistance	Very fragile	Strong	Strong	Strong	Strong	Fragile
Electrical conductivity	Yes	No	Yes	Yes	No	No
Major elements	C, (O)/Cu	C, N, O	Al, (O)	Ag, (O)	Si, B, (O)	SiO_2
Blank image	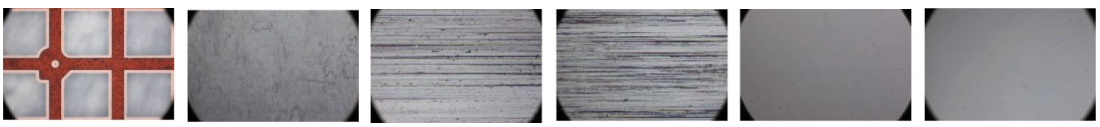					

techniques, such as scanning electron microscopy-energy dispersive X-ray spectroscopy (SEM/EDX), TEM/EDX, and/or RMS, are applied for the characterization of the same individual particles (Eom *et al.*, 2014).

When "genuine" (or nascent) NaCl sea-salt aerosols react with nitrogen oxides in the atmosphere, $NaNO_3$ species can be formed, resulting in Cl loss (Gibson *et al.*, 2006). Laboratory-generated, micrometer-sized NaCl and $NaNO_3$ mixture particles at nine mixing ratios (mole fractions of NaCl (X_{NaCl}) = 0.1 to 0.9) were examined systematically to observe their hygroscopic behavior (Gupta *et al.*, 2015b). Stepwise phase transitions were observed during the hygroscopic processes, and thus this observation can have important atmospheric implications (Wang and Laskin, 2014; Ault *et al.*, 2013b). As the NaCl-$NaNO_3$ mixture aerosol particles can maintain an aqueous phase over a wider RH range than pure NaCl particles as the SSA surrogate, it makes their heterogeneous chemistry more probable (Gupta *et al.*, 2015b). The aqueous surface region is crucial for atmospheric heterogeneous chemistry as heterogeneous reactions with gas phase species, such as N_2O_5 (Ryder *et al.*, 2014; Ault *et al.*, 2013a) or organics (Wang and Laskin, 2014), can be promoted due to the facile gas-particle partitioning (Woods *et al.*, 2012). X-ray elemental mappings using SEM/EDX indicated that the effloresced NaCl-$NaNO_3$ particles at all mixing ratios were composed of a homogeneously crystallized NaCl moiety in the center as shown in Fig. 4 (Gupta *et al.*, 2015b). Aqueous moieties of particles were reported to effloresce more easily by the heterogeneous nucleation in the presence of seeds. The formation of the core-shell type were reported for a range of binary mixed aerosol particles, such as NaCl-KCl, KCl-KI, and $(NH_4)_2SO_4$-NH_4NO_3 system (Ge *et al.*, 1996).

An individual particle hygroscopicity (IPH) system employing an optical microscope was used for a hygroscopic behavior study of field-collected aerosol particles such as Asian dust and haze particles to better understand their physicochemical properties (Li *et al.*, 2014b). Most of haze particles dissolved at RH = 68–70%, due to the presence of dominant sulfates, nitrates, and organics. Some particles collected during an Asian dust storm

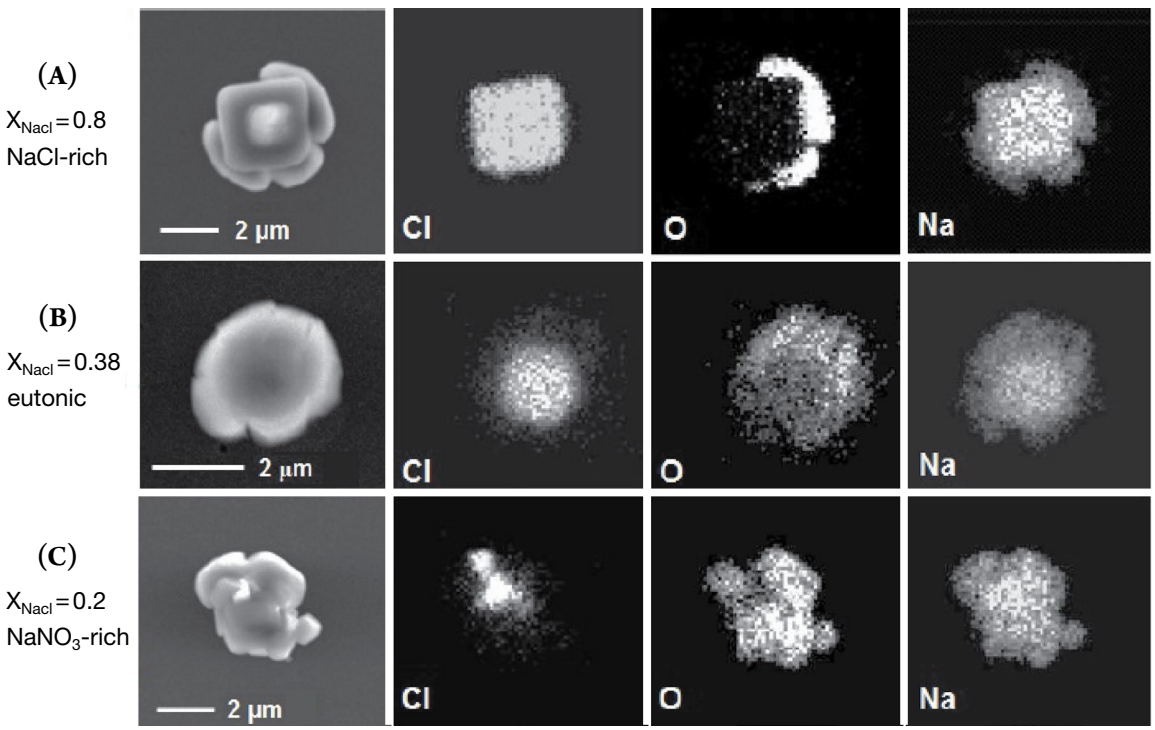

Fig. 4. Secondary electron images (SEIs) and elemental X-Ray maps obtained from SEM/EDX for Cl (from NaCl), O (from $NaNO_3$), and Na of the effloresced NaCl-$NaNO_3$ mixture particles with compositions of (A) X_{NaCl} = 0.8 (NaCl-rich); (B) X_{NaCl} = 0.38 (eutonic); and (C) X_{NaCl} = 0.2 ($NaNO_3$-rich). Reprinted with permission from Gupta, D., Kim, H., Park, G., Li, X., Eom, H.J., Ro, C.U., Atmos. Chem. Phys. 15, 3379–3393, 2015. Copyright Author(s) 2015. The Creative Commons Attribution 3.0 License (https://creativecommons.org/licenses/by/3.0/).

showed DRH = 73–75% due to the presence of external sea salt mixture. The transformation of $CaCO_3$ to $Ca(NO_3)_2$ was also observed, changing the hydrophobic dust particles to the hydrophilic ones in the continental region (Li *et al.*, 2014b). The hygroscopicity of aerosol particles collected at Mt. Lu, an acid precipitation area, measured by the IPH system showed that individual particles started to deliquesce at RH = 73–76% and finished the deliquescence at RH = 80% due to the presence of dominant NH_4^+ and SO_4^{2-} ions (Li *et al.*, 2014a). In addition, soluble organic coatings on secondary particles lowered initial DRH of particles to 63–73%, and yet with the complete dissolution at RH = 80%. Given the ambient RH of 65–85%, the secondary particles were supposed to be in the liquid phase or liquid-solid multiphase in the air (Li *et al.*, 2014a). The hygroscopic measurements on the standard ammonium sulfate (AS) and ammonium nitrate (AN) mixture particles and the individual particles collected during haze events were also conducted using the IPH system (Sun *et al.*, 2018). AS and AN particles comprise the major components of urban fine aerosols and their heterogeneous reactions in aqueous phase can accelerate the haze formation in China (Sun *et al.*, 2018). AS-AN particles showed two-stage deliquescence and single-stage efflorescence during humidification and dehydration processes, respectively. As for urban haze particles, they displayed a solid core and aqueous shell at RH = 60–80% and aqueous phase at RH > 80% during humidification, and it was concluded that most haze particles exist as the core-shell structure. The liquid water around the particles can provide an important surface for further heterogeneous reactions, forming secondary aerosols more easily in the polluted air (Li *et al.*, 2019). As particles emitted from residential coal burning are an important contributor to air pollution, the IPH system was also performed for hygroscopic measurement of these fine primary particles (Zhang *et al.*, 2018). Organic matter (OM), OM-S (sulfur-containing OM), soot-OM, S-rich, metal, and mineral particles are the major species for the coal-burning emitted particles. OM and soot particles from residential coal burning exhibited extremely low hygroscopicity, while inorganic sulfate salts or a mixture of sulfates and chlorides within individual particles can completely change the hygroscopicity of soot and OM particles, inducing a dramatic growth in size at RH = 68–85% as shown in Fig. 5 (Zhang *et al.*, 2018). The IPH system was also used for observing the hygroscopic growth of fresh primary biological aerosol particles (PBAPs), showing that the fresh PBAPs displayed low hygroscopicity (Li *et al.*, 2020). TEM measurements for these aerosol samples confirmed the chemical compositions of the particles (Li *et al.*,

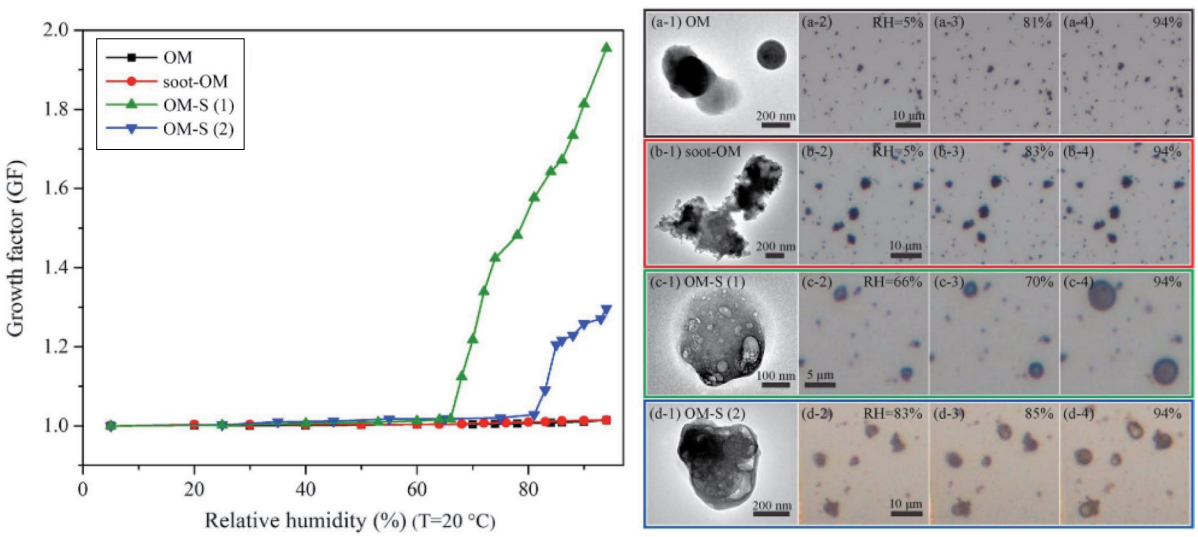

Fig. 5. Hygroscopic growth curves of particles emitted from residential coal burning as a function of relative humidity (RH). The left panel shows the growth factor (GF) of organic matter (OM), soot-OM, OM-S (1), and OM-S (2) according to RH change with the temperature of 20°C. The right panel shows TEM images of typical particles in four samples and optical images of the corresponding samples with increasing RH from 5% to 94%. Reprinted with permission from Zhang, Y., Yuan, Q., Huang, D., Kong, S., Zhang, J., Wang, X., Lu, C., Shi, Z., Zhang, X., Sun, Y., Wang, Z., Shao, L., Zhu, J., Li, W., J. Geophys. Res. Atmos. 123, 12,964–12,979, 2018. Copyright 2018 The Authors. The Creative Commons Attribution-Non-Commercial-NoDerivs License.

2020, 2014a, b; Sun *et al.*, 2018; Zhang *et al.*, 2018) and the exemplar particle images are shown in Fig. 5.

2.2 Atomic Force Microscopy (AFM)

Atomic force microscopy (AFM) is a popular technique in surface science, with a very high spatial resolution down to a nanometer level, providing 3-D imaging including size, phase, and height information by scanning the specimen surface with a sharp tip (probe) at the end of a cantilever, which can be operated under ambient conditions (Tang *et al.*, 2019, 2016a; Dazzi and Prater, 2017; Li *et al.*, 2016; Laskina *et al.*, 2015a, b; Morris *et al.*, 2015; Ghorai *et al.*, 2014; Lehmpuhl *et al.*, 1999). The technique, however, has been traditionally limited by its incapacity to offer chemical information of single particles (Li *et al.*, 2016). The coupling of chemical information with AFM, such as IR and Raman spectrometry, is expected to expand the utility of the technique (Ault and Axson, 2017; Dazzi and Prater, 2017; Wang *et al.*, 2017a; Dazzi *et al.*, 2012; Freedman *et al.*, 2010).

The hygroscopicity of both laboratory-generated and field-collected particles were examined by AFM. The structures formed on the (100) cleavage surface of NaCl in respect to RH change were studied using AFM (Dai *et al.*, 1997). A uniform layer of water was observed to be formed on the surface of the NaCl crystal when RH > 35%, and the surface with the uniform water layer evolved slowly until RH = 73%, where the water layer structure disappeared due to the deliquescence. The AFM technique, which can provide information on the surface of the particles, successfully observed that the salt surfaces can be covered with water even though RH is far below the DRH, which may not be captured by other techniques (Dai *et al.*, 1997). Similar observations were reported in a study for NaCl nanoparticles using non-contact environmental AFM (e-AFM), suggesting that the deliquescence of NaCl nanoparticles is more complex than an abrupt first-order phase transition (Bruzewicz *et al.*, 2011). AS particles collected at the North Atlantic Ocean were investigated by the combined use of AFM and TEM (Pósfai *et al.*, 1998). Accurate airborne volume of hydrated AS particles can be obtained under ambient conditions through 3-D morphological information using AFM. Supplementary TEM data on the same particles showed that the particle volume is four times smaller than that from AFM due to the loss of water when they were exposed to TEM vacuum chamber. AFM was used to quantify the shape of fine and ultrafine ambient aerosol particles by height-to-diameter ratios, based on that the phase of ambient aerosol particles could be determined (Wittmaack and Strigl, 2005). The growth factor (GF) of particles deposited on substrates was traditionally monitored by 2-D analysis of area changes responding to RH changes, assuming the droplets grow equally in all directions, which may not be true when the hygroscopic growth is not isotropic in height and diameter (Morris *et al.*, 2016). AFM was established as a reliable and accurate method to determine GFs of substrate-deposited, individual submicrometer particles through a 3-D view including both height and area, so that the volume of each particle can be obtained in a wide range of RH at ambient conditions to derive humidification and dehydration curves (Morris *et al.*, 2016). The 3-D analysis results using AFM for the atmospheric relevant particles such as NaCl, malonic acid, and their binary mixture system were compared with those obtained by 2-D analysis and the substrate-free HTDMA. As shown in Fig. 6, the AFM-determined 3-D volume-equivalent GF of the mixed

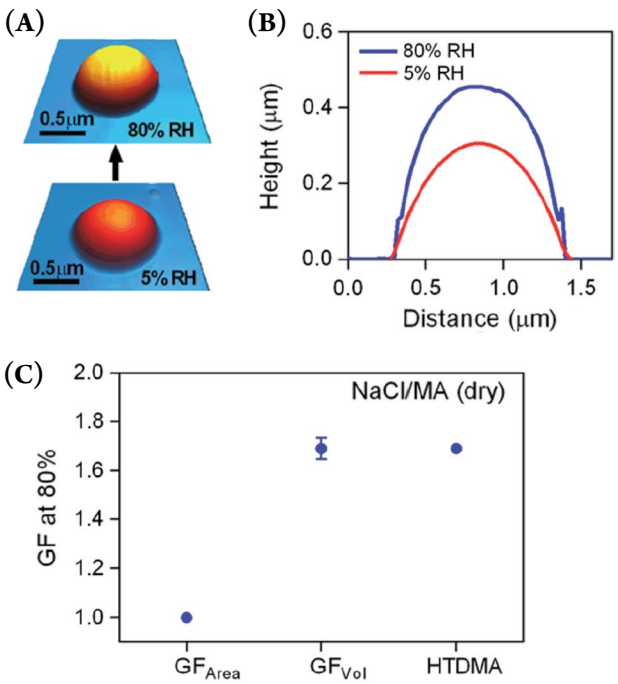

Fig. 6. Dry-deposited mixture particle of NaCl and MA. (A) 3-D Atomic Force Microscopy (AFM) images of the particle at 5% and 80% RH. (B) Cross-section of the particle at 5% RH (red) and 80% RH (blue). (C) Comparison of GF determined with area, volume, and HTDMA approaches. Reprinted with permission from Morris, H.S., Estillore, A.D., Laskina, O., Grassian, V.H., Tivanski, A.V., Anal. Chem. 2016, 88, 3647–3654. Copyright 2016 American Chemical Society.

NaCl and MA particle agreed well with that from the substrate-free HTDMA method, while that determined by 2-D area analysis was biased (Morris *et al.*, 2016).

2.3 Environmental SEM and TEM (ESEM and ETEM)

Simultaneous measurements of hygroscopic behavior and chemical compositions, mixing states, and morphology of individual particles can be performed using environmental SEM and TEM (ESEM and ETEM) which are powerful for the investigation of hygroscopic behavior of ambient aerosol particles with diameters down to approximately 100 nm (Adachi *et al.*, 2011; Freney *et al.*, 2010, 2009; Shi *et al.*, 2008; Semeniuk *et al.*, 2007a; Wise *et al.*, 2007; Hoffman *et al.*, 2004; Ebert *et al.*, 2002). The hygroscopic behavior of individual particles can be obtained based on high resolution secondary/transmission electron images showing morphological change in respect to RH change. The elemental compositions of individual particles can be obtained from EDX spectral analysis.

2.3.1 ESEM

SEM can provide detailed information on the surface of individual aerosol particles (Li *et al.*, 2016). ESEM with a spatial resolution of 8–15 nm was used to analyze the hygroscopicity of inorganic salt and soot particles (Ebert *et al.*, 2002). The hygroscopic behavior of the inorganic salts was generally consistent with the previous literature results and the activation of soot particles was also observed using the high-resolution ESEM. Gaseous HNO_3 can react with $CaCO_3$ particles, resulting in the production of hygroscopic $Ca(NO_3)_2$ species, which was observed as liquid droplets using ESEM (Shi *et al.*, 2008; Laskin *et al.*, 2005; Krueger *et al.*, 2004). The ESEM measurement for $NaNO_3$ particles showed that they exist as metastable, amorphous solids with droplet-like structure at low RH and undergo continuous growth with increasing RH as shown in Fig. 7 (Hoffman *et al.*, 2004). $(NH_4)_2SO_4$ particles of 1–2 μm size were examined using ESEM by filling the sample chamber with water vapor at a pressure of 600 Pa and with a cooling stage controlling the RH inside the chamber (Matsumura and Hayashi, 2007). The $(NH_4)_2SO_4$ droplets were observed to experience hygroscopic growth when RH was increased from 80% to 98% (Matsumura and Hayashi, 2007). The GFs of the $(NH_4)_2SO_4$ droplets were obtained by calculating the diameters, which were consistent with the theoretically estimated values, indicating the validity of the ESEM technique. The hygroscopic behavior of individual aerosol particles in Ni refineries was investigated by ESEM. Thin surface coatings of sulfates on insoluble Ni compounds were observed for some particles, which might have some implications for health assessments (Inerle-Hof *et al.*, 2007). Individual agriculture aerosol particles were characterized for their morphological, hygroscopic, and chemical properties using ESEM (Hiranuma *et al.*, 2008). Most of the particles exhibited low water uptake when exposed to up to 96% RH and a small fraction of particles in the coarse mode showed DRH = ~75–80% and reached twice their original sizes at RH = 96% due to the presence of K-salts (Hiranuma *et al.*, 2008). ESEM was utilized to examine the water uptake by individual pollen particles, a kind of primary biological aerosols (PBAs), as a function of RH, and it was observed that the surface of pollen is wettable at high sub-saturated humidity, suggesting that the pollen grains can readily act as cloud condensation nuclei even though they are only slightly hygroscopic (Griffiths *et al.*, 2012; Pope, 2010).

2.3.2 ETEM

TEM can analyze nano-sized particles and observe their internal mixing state due to its excellent spatial resolution down to 1 nm (Tang *et al.*, 2019; Li *et al.*, 2016). ETEM was used for investigating the hygroscopic behavior of ambient particles after being validated for standard salt particles such as NaBr, CsCl, NaCl, $(NH_4)_2SO_4$, and KBr (Adachi *et al.*, 2011; Freney *et al.*, 2010, 2009; Wise *et al.*, 2009, 2007, 2005; Semeniuk *et al.*, 2007a, b). The hygroscopic behavior of carbonaceous particles (soot, tar balls, and particles internally mixed with S-, K-, Mg- or Na-rich inorganic species) from biomass burning showed that soot and tar balls did not take up water, whereas the mixed organic-inorganic particles took up water at RH = 55–100%, depending on the compositions of their water-soluble phase (Semeniuk *et al.*, 2007b). The deliquescence behavior of atmospheric particles such as sulfate-coated NaCl/silicate aggregates, sulfate-coated sea-salt particles, and Mg-rich, chloride-coated sea-salt particles was observed by ETEM (Semeniuk *et al.*, 2007a). The particles started to uptake water at RH = 50–60% and deliquescent spheres appeared RH = 70–76%, indicating that the water uptakes below and above RH = 76% were due to the coating components and NaCl, respectively, when particles underwent a multi-step deliquescence process. The deliquescence and efflorescence

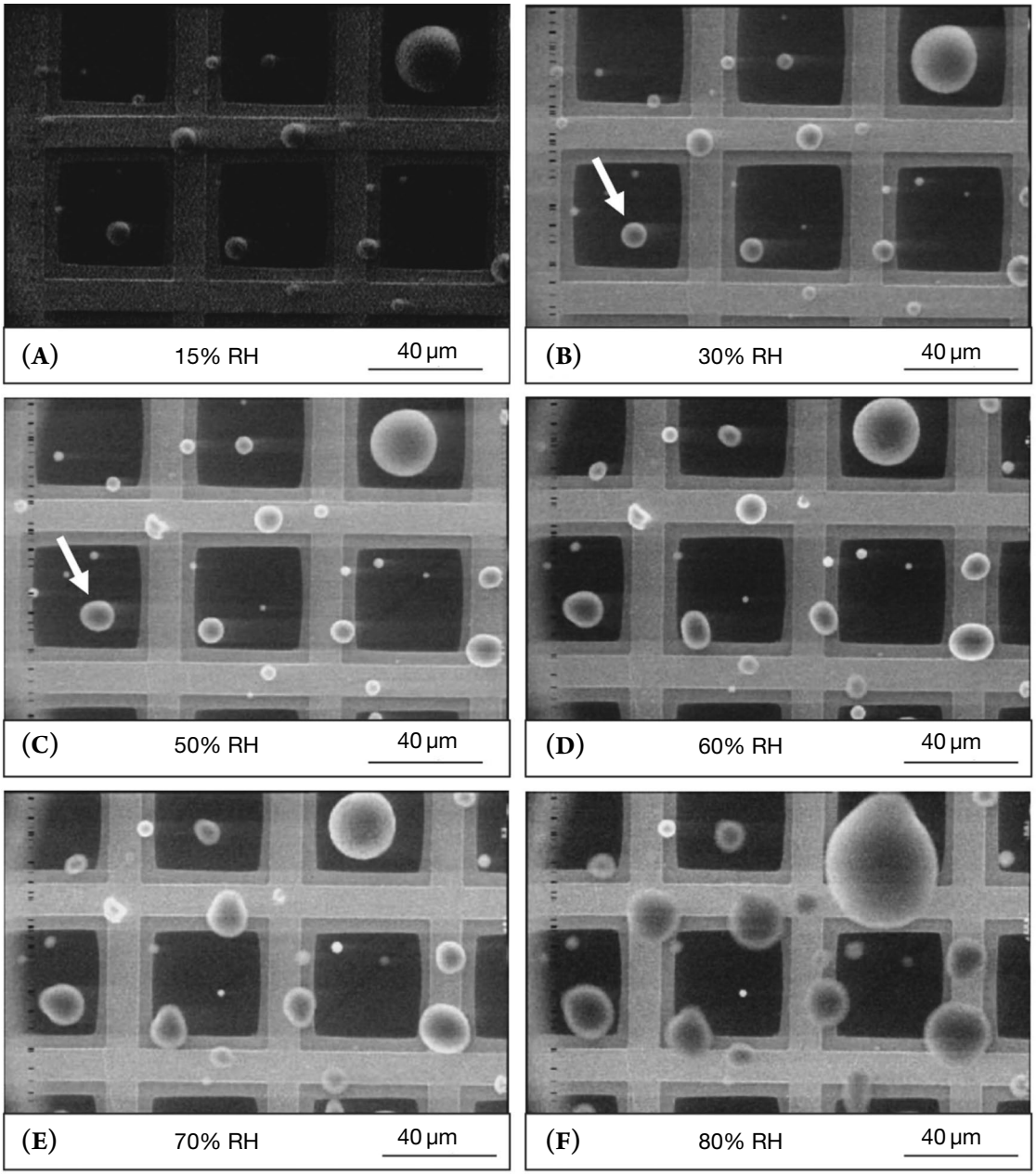

Fig. 7. Environmental SEM (ESEM) images of $NaNO_3$ aerosol particles according to RH change from (A) RH = 15% to (F) 80%. Reprinted with permission from Hoffman, R.C., Laskin, A.,Finlayson-Pitts, B.J., J. Aerosol Sci. 35(2004) 869–887. Copyright 2004 Elsevier Ltd. All rights reserved.

of K-containing particles, such as KCl, KNO_3, and K_2SO_4, and their mixtures related to biomass burning emissions were investigated using ETEM (Freney *et al.*, 2009). Some internally mixed aerosol particles with various hygroscopic properties were examined by ETEM to observe solid inclusions present inside aqueous droplets at high RH (e.g., > 65%) as shown in Fig. 8 (Freney *et al.*, 2010). Such core-shell structures have strong ability to scatter light (Adachi *et al.*, 2011; Freney *et al.*, 2010).

2.4 Scanning Transmission X-ray Microscopy (STAM)

Scanning transmission X-ray microscopy coupled with near-edge X-ray absorption fine structure spectroscopy

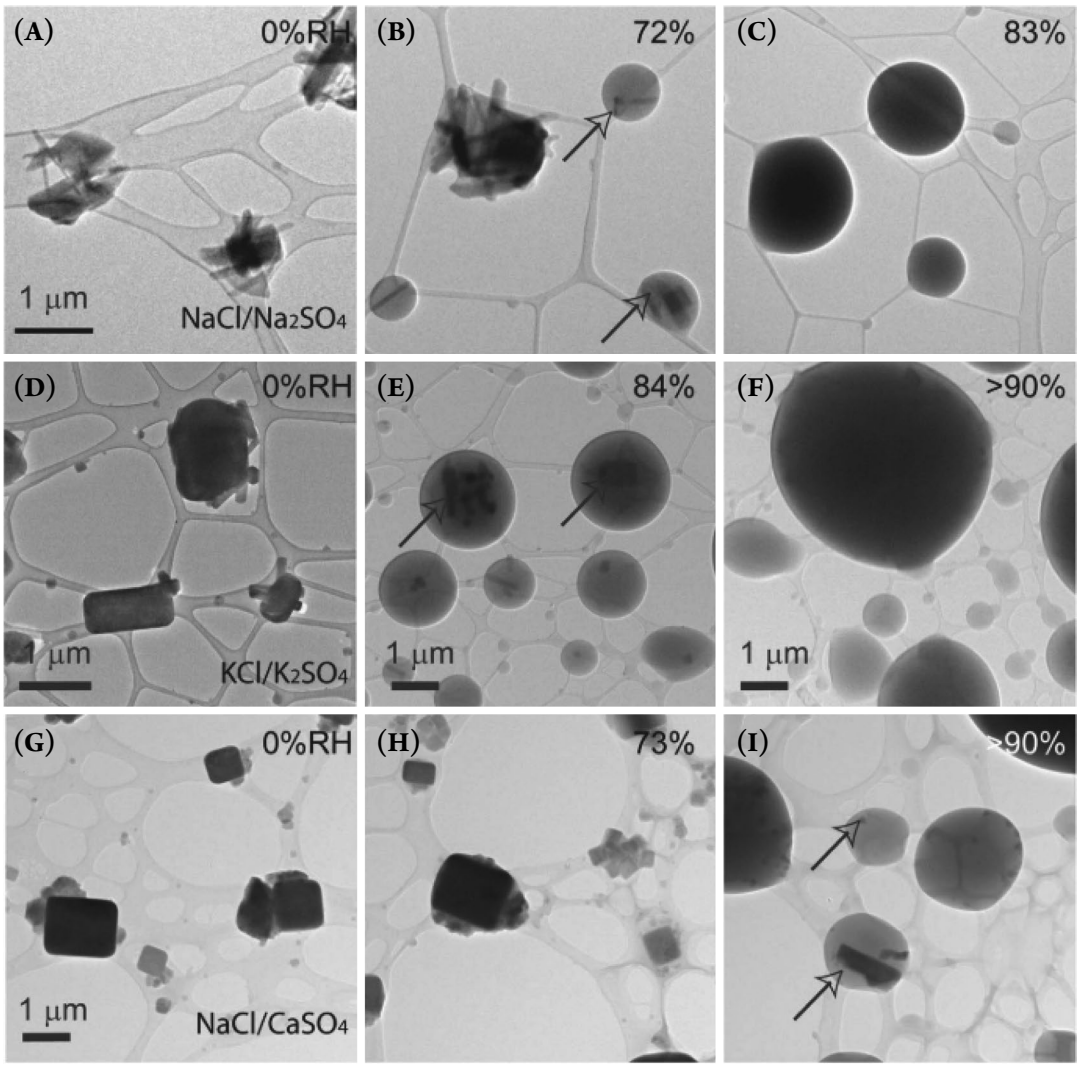

Fig. 8. TEM images of particles generated from equimolar solutions of (A–C) NaCl and Na_2SO_4, (D–F) KCl and K_2SO_4, and (G–I) NaCl and $CaSO_4$ as a function of RH. Arrows point out solid cores inside droplets. Reprinted with permission from Freney, E.J., Adachi, K., Buseck, P.R., J. Geophys. Res., 115, D19210, 2010. Copyright 2010 American Geophysical Union.

(STXM/NEXAFS) is a promising technique due to its capability for chemical imaging on a spatial resolution of 40 nm and it can determine local chemical environments within single submicron particles and heterogeneous materials (Tang *et al.*, 2019; Ault and Axson, 2017; Li *et al.*, 2016; Kelly *et al.*, 2013; Krieger *et al.*, 2012). In addition, less beam damage is induced compared to SEM and TEM as soft X-rays are probed to the sample, making it uniquely capable of quantitative analysis of light elements (such as C, N, O) (Moffet *et al.*, 2011; de Smit *et al.*, 2008; Maria *et al.*, 2004). Hygroscopic properties of individual submicrometer AS particles were measured using STXM/NEXAFS and the results were reported to be consistent with previous literature results (Zelenay *et al.*, 2011). The STXM/NEXAFS technique was further used to study the morphology of AS/adipic acid mixture particles by examining spectral features at both carbon and oxygen edges as a function of RH and the heterogeneous distributions of the mixtures under both dry and wet conditions were reported (Zelenay *et al.*, 2011). STXM/NEXAFS was used to observe hygroscopic growth and chemical change of fine malonic acid particles according to RH change (Ghorai *et al.*, 2011). Hygroscopic GFs, which were obtained from water-to-solute ratios (WSRs) based on STXM/NEXAFS and micro-FTIR data, agreed well with previous data reported in the liter-

ature. The efficient keto-enol tautomerization of malonic acid was observed with the enol form dominating at high RH. A compact gas-phase reactor for performing in situ STXM was assembled for the measurement under water vapor, which provided a more stable condition for the hygroscopic study (Kelly *et al.*, 2013). The setup was calibrated by examining NaBr, NaCl, $(NH_4)_2SO_4$, and KCl with different DRH values. A following study using the reactor coupled to STXM was performed to measure the mass-based hygroscopicity of atmospheric particles and characterize their elemental and carbon functional group compositions simultaneously (Piens *et al.*, 2016). The setup was firstly used to measure hygroscopic behavior of laboratory generated NaCl, NaBr, KCl, $(NH_4)_2SO_4$, levoglucosan, and fructose particles and the results agreed well with those calculated from AIOMFAC. Field-collected atmospheric particles with unknown compositions were then determined by in-situ STXM/NEXAFS and SEM/EDX and particles with Na and Cl contents were observed to have high hygroscopicity (Piens *et al.*, 2016). The dependence of shikimic acid ozonolysis on the humidity and thereby viscosity was investigated by in-situ STXM/NEXAFS, showing that the degradation kinetics of shikimic acid depend on the relative humidity, which in turn are influenced by the increased viscosity of the shikimic acid-water mixture (Steimer *et al.*, 2014). STXM/NEXAFAS was also applied to investigate field-collected particles under controlled water vapor environment. For example, the hygroscopic behavior of aerosol particles collected during an anthropogenic polluted period at the Amazonian rain forest which were internally mixed with carbonaceous (such as secondary organic aerosols and soot) and inorganic (such as ammonium sulfate) components was analyzed using STXM/NEXAFAS (Pöhlker *et al.*, 2014). Efflorescence during the humidification was claimed to occur as the impacted ambient organic-inorganic mixture aerosols initially had amorphous or poly-crystalline structures and underwent restructuring through kinetic water and ion mobilization, resulting in the crystallization of inorganic salts during the humidification (Pöhlker *et al.*, 2014). As shown in Fig. 9, cubic structures in Fig. 9B and F suggest that sulfate salts crystallized upon the humidification. Highly absorbing spots in carbon maps represent soot particles, which were incorporated in amorphous inorganic material (i.e., ammonium sulfate) and localized on the surface of inorganic crystals (white arrows in Fig. 9H) at 0% and 80% RH, respectively (Pöhlker *et al.*, 2014).

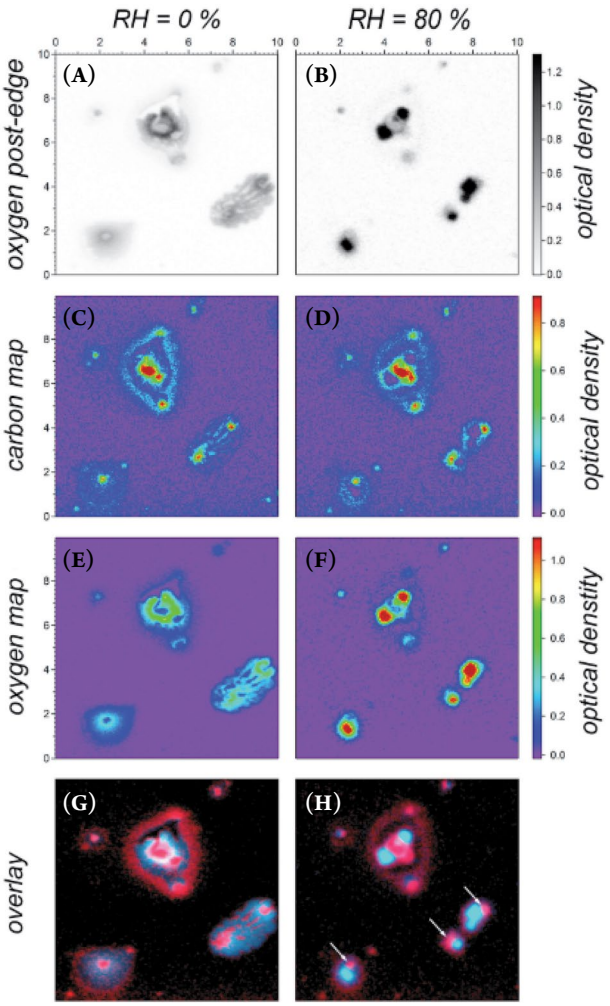

Fig. 9. Scanning Transmission X-ray Microscopy (STXM) images and elemental maps of representative ambient organic-inorganic mixed particles subjected to increasing RH. (A and B) Oxygen post-edge images, (C and D) carbon elemental maps, (E and F) oxygen maps, and (G and H) overlay of carbon and oxygen map (C = red, O = blue). Reprinted with permission from Pöhlker, C., Saturno, J., Krüger, M. L., Förster, J.-D., Weigand, M., Wiedemann, K.T., Bechtel, M., Artaxo, P., Andreae, M.O., Geophys. Res. Lett., 41, 3681–3689, 2014. Copyright 2014 American Geophysical Union.

3. SPECTROSCOPIC STUDIES

Vibrational spectroscopic techniques such as Raman and FTIR spectroscopies can be quite powerful for the hygroscopicity study of individual aerosol particles when an environmental cell, named in-situ system, is installed

because the spectroscopic techniques can provide real-time chemical compositional evolution based on functional groups of individual particles during hygroscopic measurements (Wu *et al.*, 2019; Li *et al.*, 2017; Wang *et al.*, 2017b; Yeung *et al.*, 2009; Lee *et al.*, 2008; Liu *et al.*, 2008b; Reid *et al.*, 2007; Li *et al.*, 2006). A built-in or coupled optical microscope can also be used for observing morphological change of individual particles during hygroscopic measurements (Li *et al.*, 2017; Gupta *et al.*, 2015a). Both spectral and optical image information can be used to investigate the hygroscopic behavior of individual particles including the determination of DRH and ERH values. In addition, the vibrational spectra obtained during hygroscopic measurements can provide detailed information on chemical functional groups, molecular interactions, and particle phase to allow better understanding of the hygroscopic behavior of complex aerosol particles (Li *et al.*, 2017; Wang *et al.*, 2017b; Lee *et al.*, 2008).

3.1 In-situ Raman Microspectrometry (RMS)

Individual single salt, mixed, or ambient aerosol particles collected on a variety of substrates have been examined by in-situ Raman micro-spectrometry (RMS) (Baustian *et al.*, 2012; Baustian *et al.*, 2010; Ciobanu *et al.*, 2009; Treuel *et al.*, 2009; Yeung *et al.*, 2009; Liu *et al.*, 2008b; Li *et al.*, 2006). Hygroscopic properties of individual $MgSO_4$ and $NaNO_3$ droplets deposited on a quartz substrate were investigated based on Raman spectral evolution in respect to RH change (Wang *et al.*, 2005; Li *et al.*, 2006). The hygroscopic behavior of individual $Ca(NO_3)_2$ and internally mixed $Ca(NO_3)_2$/$CaCO_3$ particles deposited on Teflon film was investigated using RMS (Liu *et al.*, 2008b). The RH dependence of the water-to-solute ratio (WSR) was quantified for $Ca(NO_3)_2$ and the phase transitions were successfully determined by Raman spectral analysis related to chemical structure evolution. The different hygroscopic behavior and phase transitions of AS-adipic acid particles with various mixing ratios deposited on a hydrophobic substrate were studied using RMS, and the hygroscopic behavior of the AS fraction in the mixed particles was found not to be much influenced by the organic moiety (Yeung *et al.*, 2009). The similar setup was later used to determine the hygroscopicity and phase transitions of AS, AN, malonic acid (MA), glutaric acid (GA), glyoxylic acid (GlyA), as well as two mixed particle systems AS-MA and AS-GA, and the results very well corresponded to the previous literature and model values (Yeung *et al.*, 2010; Yeung and Chan, 2010). In-situ RMS was used to observe the water uptake of the mixture aerosols composed of various inorganic and organic species, such as $Ca(NO_3)_2$ and $CaCO_3$ mixed with $H_2C_2O_4$ and dicarboxylic acids mixed with NaCl or AS (Wang *et al.*, 2017b; Ma *et al.*, 2013; Ma and He, 2012). The chemical reactions between the organic and inorganic compositions, which drastically change the chemical compositions and hygroscopic behavior of the mixtures, were found to occur based on Raman spectral analysis.

Since Cl^- is the most abundant anion in nascent sea spray aerosols (SSAs) and Na^+ and Mg^{2+} are the first and second most abundant cations, respectively, (Seinfeld and Pandis, 2016), NaCl-$MgCl_2$ binary mixture particles can be the better surrogate for the nascent SSAs than pure NaCl aerosols. Due to the major role of the $MgCl_2$ moiety in the hygroscopic behavior of the nascent SSAs, the study on the NaCl-$MgCl_2$ mixture particles may have important implications for nascent SSA heterogeneous chemistry (Ault *et al.*, 2013a; Woods *et al.*, 2010; Wise *et al.*, 2009; Liu *et al.*, 2007). An in situ RMS setup, which was composed of three parts: (A) see-through impactor, (B) Raman microscope/spectrometer, and (C) humidity controlling system, was employed for hygroscopic studies of pure $MgCl_2$ and NaCl-$MgCl_2$ mixture aerosol particles (Gupta *et al.*, 2015a). The experimental setup was similar to that used for optical microscopy, with the Raman spectrometer replacing the optical microscope (Gupta *et al.*, 2015a; Ahn *et al.*, 2010). As for the hygroscopic behavior for pure $MgCl_2$ particles, characteristic OH-stretching Raman signatures indicated the crystallization of $MgCl_2 \cdot 4H_2O$ at low RH as shown in Fig. 10, suggesting that the kinetic barrier to the more stable $MgCl_2 \cdot 6H_2O$ crystallization was not overcome in the timescale of the dehydration measurements (Gupta *et al.*, 2015a). The kinetic barrier to $MgCl_2 \cdot 6H_2O$ could be overcome when there was sufficient condensed water for optimally sized crystalline NaCl acting as heterogeneous nucleation seeds.

The hygroscopicity of AS and AN mixture particles was studied theoretically and experimentally (Ling and Chan, 2007; Ge *et al.*, 1998) although their hygroscopic behavior has been under no comprehensive understanding. In-situ RMS measurements on pure AS, AN, and AS-AN mixture aerosol particles with various mixing ratios were performed (Wu *et al.*, 2019). Two types of

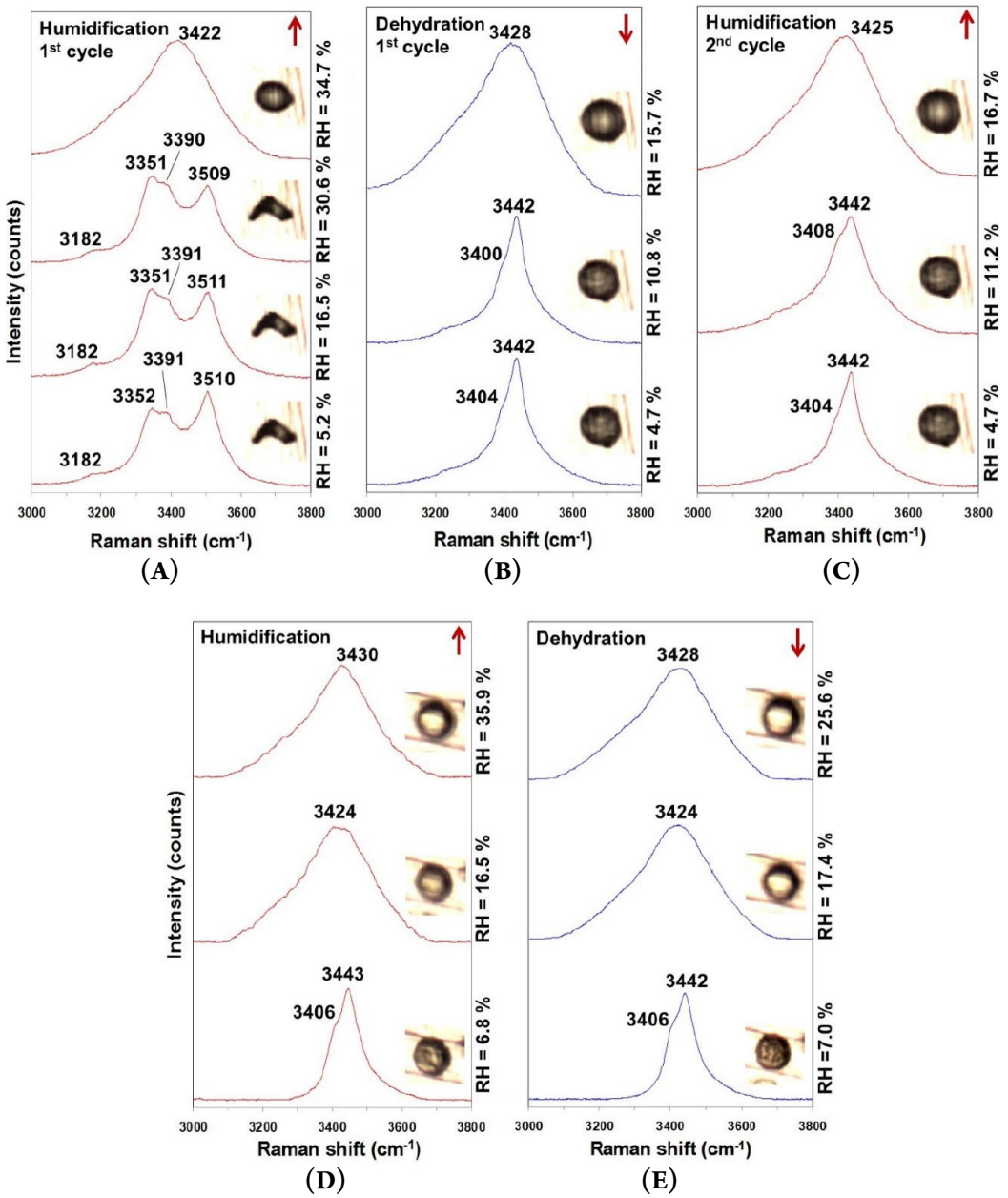

Fig. 10. Optical images and corresponding Raman spectra obtained by in situ RMS, for a representative dry-deposited $MgCl_2 \cdot 6H_2O$ particle during (A) humidification (first cycle), (B) dehydration (first cycle), and (C) humidification (second cycle) processes and for a representative wet-deposited $MgCl_2$ particle during (D) humidification and (E) dehydration processes. Reprinted with permission from Gupta, D., Eom, H.J., Cho, H.R., Ro, C.U., Atmos. Chem. Phys., 15, 11273–11290, 2015. Copyright Author(s) 2015. The Creative Commons Attribution 3.0 License (https://creativecommons.org/licenses/by/3.0/).

hygroscopic behavior of pure AN particles are shown in Fig. 11. The AS and AN mixture droplets can crystallize as the mixtures of pure AS crystal and stable and/or metastable double salts (2AN · AS and 3AN · AS, respectively) and the degree of metastability might differ under different conditions (Ling and Chan, 2007). Hygroscopic growth, corresponding optical images, and Raman spectra at specific RHs of a particle of mole fraction of AS (X_{AS}) = 0.6 is shown in Fig. 12 as an example (Wu *et al.*, 2019). During the humidification process, the size and shape of the particles remained constant until a slight decrease in size was observed at RH = 60–68.5%, which

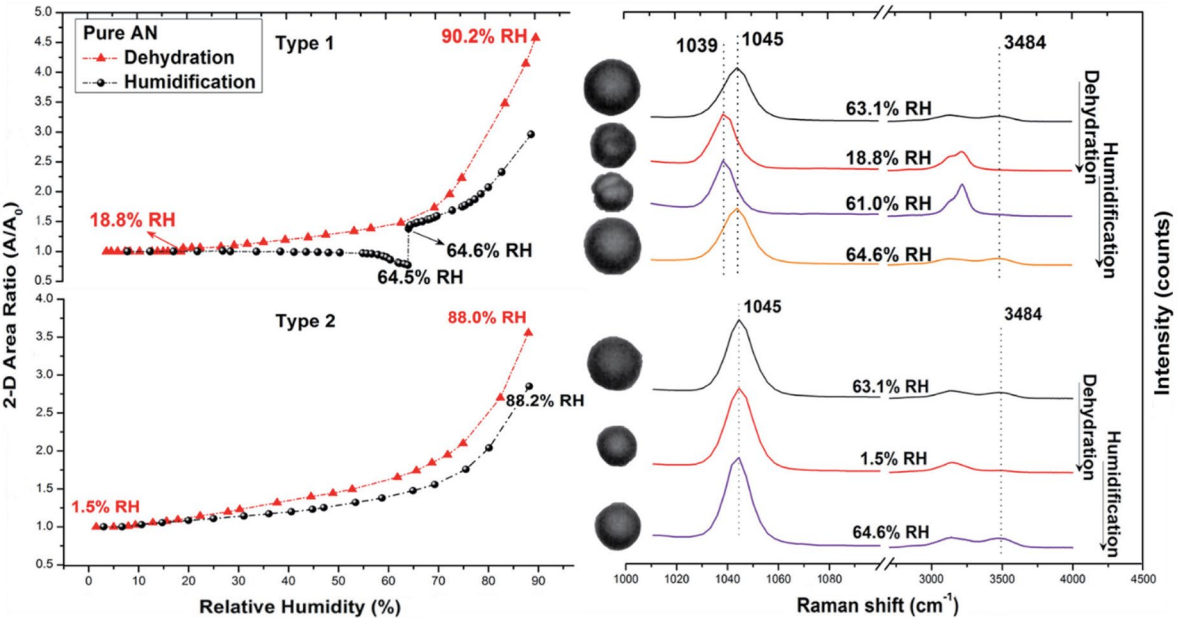

Fig. 11. Hygroscopic curve, corresponding optical images, and Raman spectra at specific RHs of two types of AN particle. The recorded transition RHs in both dehydration and humidification processes are marked with arrows in the hygroscopic curve. Reprinted with permission from Wu, L., Li, X., Ro, C.-U., Asian J. Atmos. Environ, 13, 3, 196–211, 2019. Copyright 2019 by Asian Journal of Atmospheric Environment. The Creative Commons Attribution Non-Commercial License (http://creativecommons.org/licenses/by-nc/4.0/).

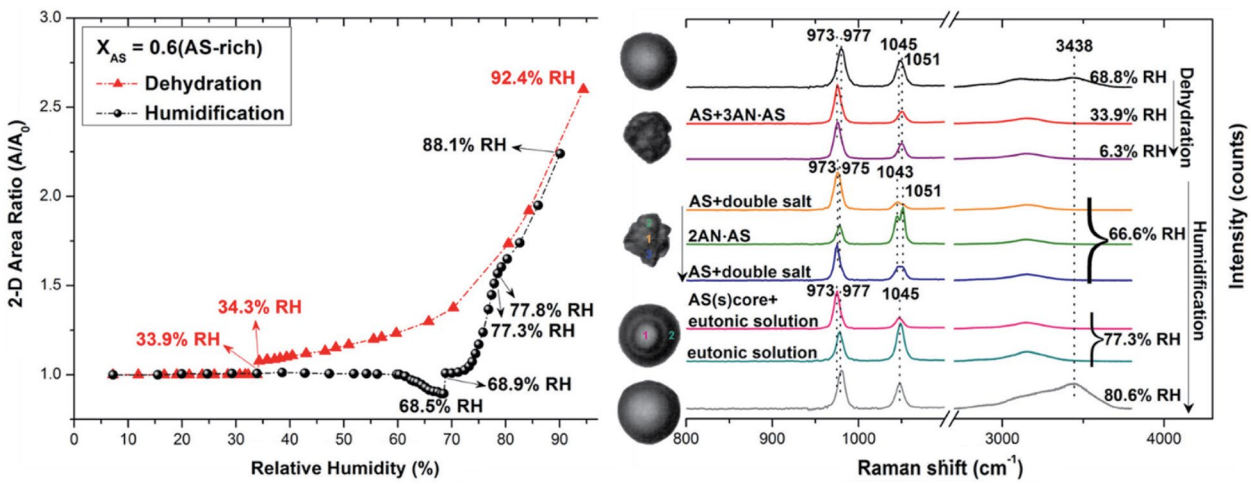

Fig. 12. Hygroscopic curve, corresponding optical images, and Raman spectra at specific RHs of an AS-rich particle ($X_{AS} = 0.6$). The recorded transition RHs in both dehydration and humidification processes are marked with arrows in the hygroscopic curve. Reprinted with permission from Wu, L., Li, X., Ro, C.-U., Asian J. Atmos. Environ, 13, 3, 196–211, 2019. Copyright 2019 by Asian Journal of Atmospheric Environment. The Creative Commons Attribution Non-Commercial License (http://creativecommons.org/licenses/by-nc/4.0/).

is also seen in the optical image of the particle at RH = 66.6%. Three Raman spectra at RH = 66.6% were obtained at different positions on the particle. As shown in the middle green-colored Raman spectrum which is for the upper part of the particle, the NO_3^- peak at RH = 66.6% showed double peaks at 1043 and 1051 cm^{-1}, indicating the transformation of a metastable 3AN·AS to a stable 2AN·AS double salt (Ling and Chan, 2007). The

center and bottom parts of the particle (the orange- and blue-colored Raman spectra, respectively) seemed to be the mixture of pure AS and double salt crystals as the pure AS crystal peak at 973 cm^{-1} and the double peaks at 1043 and 1051 cm^{-1} were observed. It seems that heterogenous chemical distributions occurred during the structural rearrangement at RH = 60–68.5%. The particle showed a first partial deliquescence transition at RH = 68.9%, which is the DRH of the eutonic composition. The particle had a liquid eutonic shell with a solid core structure as shown in the optical image of the particle at RH = 77.3%. Raman spectra of the center and edge parts of the particle showing the SO_4^{2-} peak at 973 and 977 cm^{-1}, respectively, indicating the solid core is a pure AS crystal. Upon the further increase in RH, the particle absorbed water and grew in size until a second deliquescence transition occurred at RH = 77.8%, i.e., a second DRH, where the AS solid core dissolved completely, after which the particle grew continuously with the further increase in RH. The AS-AN mixture particles with different mixing ratios were observed to crystallize into different forms, leading to different MDRHs and DRHs with bigger gap than those from theoretical models, which can promote their capability of probable heterogeneous chemistry on aqueous aerosol surface (Wu *et al.*, 2019).

Nascent SSAs were reported to undergo the chloride depletion mainly due to the reactions of $NaCl/MgCl_2$ with inorganic NO_x/HNO_3 and SO_x species (Ault *et al.*, 2013a; Beardsley *et al.*, 2013; Prather *et al.*, 2013; Saul *et al.*, 2006; ten Brink, 1998). Ambient SSAs were also claimed to react with water-soluble organic acids, which was driven by the liberation of gaseous HCl (Laskin *et al.*, 2012). In situ RMS analysis for the hygroscopic behavior of NaCl-malonic acid (MA) mixture aerosols with different mixing ratios clearly showed that the chemical reaction between NaCl and MA occurred rapidly and considerably, producing mono-sodium malonate. The chemical reaction was facilitated when MA is more enriched in the aerosols because the controlling factor for the reactivity of the aerosols is the availability of H^+ ions dissociated from MA (Li *et al.*, 2017).

3.2 In-situ FTIR Spectroscopy

Similar to Raman analysis, FTIR spectroscopy can be used to monitor chemical compositional changes of particles when exposed to water vapor as FTIR and Raman spectroscopies are sensitive to functional groups such as OH band (Tang *et al.*, 2019). The hygroscopicity of inorganic particles such as $(NH_4)_2SO_4$, NH_4HSO_4, NaCl, $MgCl_2$ and NH_4NO_3, and $(NH_4)_2SO_4$ mixed with organics, were investigated by transmission FTIR spectroscopy (Zawadowicz *et al.*, 2015; Braban *et al.*, 2001; Cziczo and Abbatt, 2000; Cziczo *et al.*, 1997). The transmission FTIR analysis on heterogeneous reactions of nitric acid with oxide particles of crustal elements were reported to be significantly enhanced in the presence of water vapor (Goodman *et al.*, 2001). Attenuated total reflection FTIR (ATR-FTIR) and diffusion reflectance infrared Fourier transform spectroscopy (DRIFTS) can also be used for hygroscopicity study. The hygroscopicity of $MgSO_4$ particles were studied by ATR-FTIR, in which the evolution of the SO_4^{2-} and the water O-H peaks was directly related to their hygroscopic behavior, which agreed well with the previous reports (Zhao *et al.*, 2006). ATR-FTIR was also used to monitor the water uptake and phase transitions for atmospherically relevant particles such as NaCl, $NaNO_3$, NH_4NO_3, $(NH_4)_2SO_4$, $Ca(NO_3)_2$, SiO_2, levoglucosan, oxalic acid, malonic acid, succinic acid, phthalic acid, Na-carboxylate, and fly ash particles as a function of RH (Gao *et al.*, 2018; Navea *et al.*, 2017; Jing *et al.*, 2016; Zhang *et al.*, 2014; Schuttlefield *et al.*, 2007). The spectral features including absorption band frequencies, full-width half-maximum (FWHM) of the vibrational modes, and integrated area of water stretching and bending regions can distinguish various processes such as water adsorption onto the surface, water absorption to become hydrate forms, and deliquescence to become droplets when particles uptake water vapor (Schuttlefield *et al.*, 2007). ATR-FTIR was used to investigate the supersaturation and crystallization process of $NaNO_3$-Na_2SO_4 mixture droplets deposited on ZnSe with mixing ratios of 1 : 1, 3 : 1, and 10 : 1, in which the crystals and supersaturated droplets formed during dehydration when the substrate effects were present and absent, respectively (Tong *et al.*, 2010). Temperature-dependent hygroscopic behavior of sodium methanesulfonate (CH_3SO_3Na) salt was examined using ATR-FTIR, suggesting that sea-salt particles would have quite different DRHs and ERHs depending on temperature once they reacted with methanesulfonic acid, which would have important atmospheric implications (Zeng *et al.*, 2014). IR spectra of MSA-Na particles undergoing hygroscopic growth at 296 K is shown in Fig. 13 as an example (Zeng *et al.*, 2014). As RH increases, an absorbed water IR peak is observed in the region of 3660 to 2750 cm^{-1} and gradually becomes significant at the higher RH

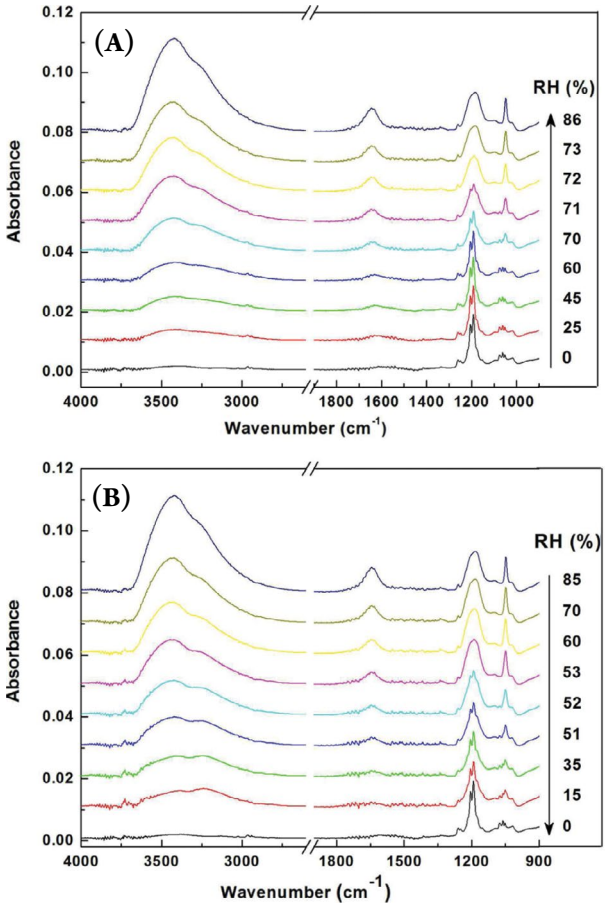

Fig. 13. IR spectra of MSA-Na particles through humidification (A) and dehydration (B) processes at 296 K. Reprinted with permission from Zeng, G., Kelley, J., Kish, J.D., Liu, Y., J. Phys. Chem. A 2014, 118, 583–591. Copyright 2014 American Chemical Society.

region. A substantial amount of water is absorbed by the solid MSA-Na particles when RH approaches 70%, after which the water band increases rapidly with increasing RH. During the dehydration process, the deliquesced MSA-Na droplets gradually lose the water with the water band decreasing accordingly until a rapid transition occurs at RH = ~52%, where particles undergo efflorescence and become crystal form again. An FTIR spectrometer coupled with optical microscope (micro-FTIR) was used to investigate the hygroscopic behavior of atmospheric relevant particles (Liu and Laskin, 2009; Liu *et al.*, 2008a; Wu *et al.*, 2007), which was claimed to agree well with that reported in previous studies. Water-to-solute ratios (WSRs) in particles as a function of RH, which were obtained from the absorbance ratio between water IR peak at 3400 cm^{-1} and the solute peak, were used to derive the hygroscopic curves. Chemical compositions and hygroscopic properties of laboratory generated NaCl particles mixed with malonic acid (MA) and glutaric acid (GA) at different molar ratios were studied using the micro-FTIR, and the formation of sodium malonate and sodium glutarate salts resulting from HCl evaporation were observed (Ghorai *et al.*, 2014). In-situ DRIFTS was demonstrated to be a reliable technique for studying the water adsorption on NaCl and mineral particles (Ibrahim *et al.*, 2018; Joshi *et al.*, 2017; Ma *et al.*, 2010). The hygroscopic behavior for MgO, α-Al_2O_3, and $CaCO_3$ particles mixed with acetic acid was analyzed with this technique (Ma *et al.*, 2012). A later study investigated heterogeneous reactions of acetic acid with γ-Al_2O_3, SiO_2, and CaO in a range of RHs using transmission FTIR. The reaction rate of acetic acid with γ-Al_2O_3 increased significantly with increasing RH, while acetic acid and water were found to compete for surface adsorption sites on SiO_2 particles (Tang *et al.*, 2016b).

3.3 Levitation Studies of Single Particles

When individual particles are levitated for the study of their hygroscopic behavior, they are free of probable heterogeneous nucleation due to no contact with solid surfaces, which makes it an effective way to explore highly supersaturated solutions and solution thermodynamics (Davis, 1997). The levitation techniques are generally categorized into electrodynamic balance, optical levitation, and acoustic levitation.

3.3.1 Electrodynamic Balance (EDB)

Electrodynamic balance (EDB) was described in detail in previous studies (Tong *et al.*, 2015; Krieger *et al.*, 2012; Lee *et al.*, 2008; Reid and Sayer, 2003; Davis, 1997). Briefly, a particle sized in 1–100 μm can be levitated inside an EDB chamber with properly adjusted AC and DC electric fields (Tang *et al.*, 2019). Fig. 14(A) shows a design of EDB with a pair of DC endcap electrodes and an AC ring electrode. A particle will be charged by induction before entering the EDB chamber, after which the electrostatic force imposed on the particle by the DC voltage balances the weight of the particle, leading to the confinement of the particle at the center of the EDB (Zhang and Chan, 2000). The mass of a particle is proportional to the DC balancing voltage (Pope, 2010). The EDB technique has been widely used for hygroscopicity studies for atmospheric relevant particles, in which mass or size changes of the levitated particles as a function of RH were used to derive the humidification and dehydration curves (Griffiths *et al.*, 2012; Haddrell *et al.*, 2012;

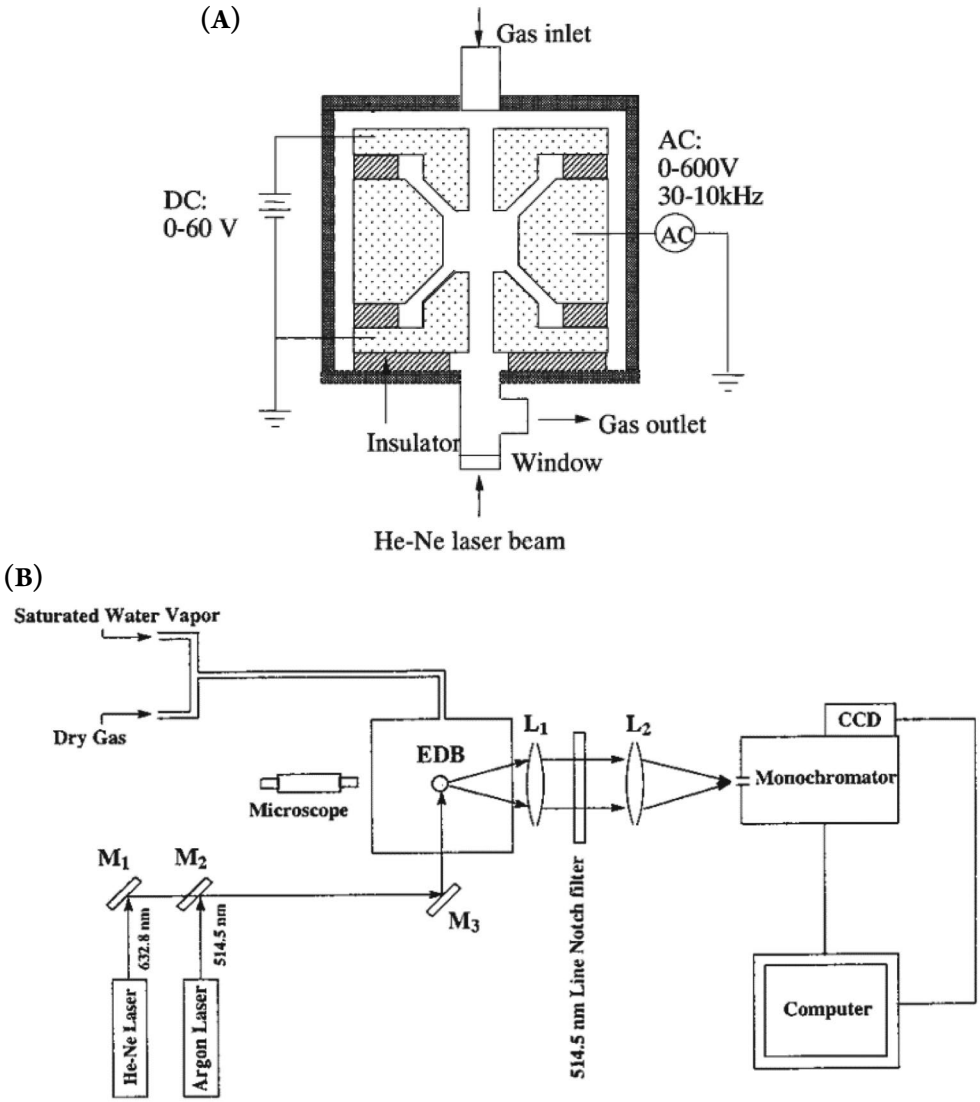

Fig. 14. Schematic diagram of electrodynamic balance (EDB) and EDB-Raman system. Reprinted with permission from (A) Zhang, Y.-H., Chan, C.K., J. Phys. Chem. A 2000, 104, 9191–9196. Copyright 2000 American Chemical Society; (B) Zhang, Y.-H., Chan, C.K., J. Phys. Chem. A 2002, 106, 285–292. Copyright 2002 American Chemical Society.

Hargreaves *et al.*, 2010; Pope, 2010; Pope *et al.*, 2010; Peng and Chan, 2001; Peng *et al.*, 2001; Tang and Fung, 1997; Tang and Munkelwitz, 1994; Cohen *et al.*, 1987a, b, c). As shown in Fig. 14(B), EDB can be combined with spectroscopic techniques such as RMS to obtain chemical evolution information according to RH change in hygroscopic studies (Zhang and Chan, 2002). Molecular structures of droplets including equal molar Na_2SO_4/$MgSO_4$ mixture, Na_2SO_4, $(NH_4)_2SO_4$, $MgSO_4$, $ZnSO_4$, and $CdSO_4$ single salts were examined using molar water-to-solute ratios (WSRs) and Raman spectra obtained at different RHs in an EDB (Zhang and Chan, 2002, 2000). The formation of contact ion pairs at high concentrations was reported based on the spectral characteristics. The combination of EDB and RMS was also used to investigate the phase transformation in AN/AS mixed particles and the hygroscopicity of organic and inorganic mixtures particles (Lee *et al.*, 2008; Ling and Chan, 2008, 2007). Changes in Raman peak positions and full width at half height (FWHH) were used to examine the molecular interactions and phase transformation (Lee *et al.*, 2008). AN/AS mixtures were reported to form the metastable 3AN·AS double salt when crystallization occurred, which gradually transformed into the stable 2AN·AS

double salt depending on RH (Ling and Chan, 2007). AS/MA (malonic acid) mixture particles remained partially crystallized at RH down to 16%, whereas AS/GA (glutaric acid) and AS/SA (succinic acid) mixture particles completely became dried at RH = ~30–36% and below, respectively (Ling and Chan, 2008). Partial deliquescence was observed at RHs of < 10% to 79%, 70% to 80%, and 80% to > 90% for the AS/MA, AS/GA, and AS/SA particles, respectively (Ling and Chan, 2008). Fig. 15 shows the Raman spectra evolution of the AS/MA particle during dehydration and humidification processes. At RH = 16%, a small portion of MA crystallized onto the AS seed as shown in Fig. 15(B) (Ling and Chan, 2008). EDB was coupled with fluorescence spectroscopy for hygroscopic measurements, where the solvated-to-free water ratios in the droplets were determined (Choi and Chan, 2005; Choi *et al.*, 2004). The solvated and free water were distributed heterogeneously in the droplets and the crystallization or supersaturation of the droplets were found to occur when their amounts become equal (Choi *et al.*, 2004). The distributions of solvated and free water in NaCl, Na_2SO_4, $(NH_4)_2SO_4$, $MgSO_4$, $Mg(NO_3)_2$, and a mixture of NaCl and Na_2SO_4 droplets were studied using EDB coupled with fluorescence spectroscopy system (Choi and Chan, 2005; Choi *et al.*, 2004).

3.3.2 Optical Levitation

The optical trapping system for particles was described well in previous studies (Tang *et al.*, 2019; Gong *et al.*, 2018; Krieger *et al.*, 2012; Wills *et al.*, 2009; Mitchem and Reid, 2008; Ashkin, 2000). Briefly, the interaction between the incident laser beam and a particle induces a scattering and a gradient force, which results in optical levitation and optical tweezer techniques, respectively, for trapping particles optically (Tang *et al.*, 2019; Krieger *et al.*, 2012). The optical levitation was achieved by overcoming the gravitational force of particles (20–100 μm) with backwards light scattering using a vertically propagating laser beam, while the optical tweezer was realized by applying a strong gradient restoring force many orders of magnitude larger than the scattering and gravitational forces of particles (1–10 μm), leading to 3-dimensional stabilization in position with a single laser beam (Krieger *et al.*, 2012). Fig. 16 shows a schematic diagram of an optical tweezer, where a trapping beam passes through two sets of beam expansion optics and it is split into two separate beams, after which the beams are focused into the sample cell through a coverslip by an oil immersion objective, allowing the two droplets to be trapped (Mitchem *et al.*, 2006c). Hygroscopicity of optically-trapped particles can be investigated when imaging and/or spectroscopic systems are combined (Tang *et al.*, 2019; Krieger *et al.*, 2012; Mitchem and Reid, 2008). Optical trapping techniques were used to examine the deliquescence and efflorescence of atmospherically relevant particles in the presence and absence of a surface-contacted seed solid, in which the contact efflorescence of the particles was reported (Davis *et al.*, 2015a, b). For optically levitated multicomponent microdroplets including glycerin, water, and ammonium sulfate, evaporation and phase transition from the liquid to the solid state of ammonium sulfate were observed by morphology-dependent resonances observed in Raman spectra (Trunk *et al.*, 1997). The hygroscopic behavior of NaCl droplet trapped in an optical tweezer was investigated by Raman spectroscopy through the variations of OH stretching band subjected to RH change (Treuel *et al.*, 2010; Mitchem *et al.*, 2006a). Stimulated Raman scattering can be used to determine the size of the trapped droplet with nanometer precision and with a time resolution of 1 s (Mitchem *et al.*, 2006a). The capability of the combination of optical tweezers and Raman spectroscopy to study the coagulation of decane and water droplets was reported (Mitchem *et al.*, 2006b). By the combined use of Raman spectroscopy and optical tweezers, mixed decane/NaCl aqueous droplets were probed for investigating their internal structures, where the decane formed a layer on the surface of the core region in aqueous droplets (Buajarern *et al.*, 2007). Hygroscopic behavior of oleic acid and NaCl mixture particles before and after ozonolysis was examined using the optical tweezer and the phase and morphology were investigated as a function of RH using a cavity enhanced Raman spectroscopy (CERS) (Dennis-Smither *et al.*, 2012). The hygroscopic behavior of NaCl was claimed not to be influenced by the organic moiety. The efflorescence promptly occurred, whereas the deliquescence was a gradual process lasting around 20 s, during which the dissolution of the inorganic component and the adoption of an equilibrium morphology occurred as shown in Fig. 17 (Dennis-Smither *et al.*, 2012). The water adsorption onto optically trapped mineral oxides under controlled RH was observed by Raman spectroscopy (Rkiouak *et al.*, 2014). The optically trapped SiO_2 particles were monitored by Raman spectroscopy for chemical composition changes when exposed to N_2O_5 flow at different RHs

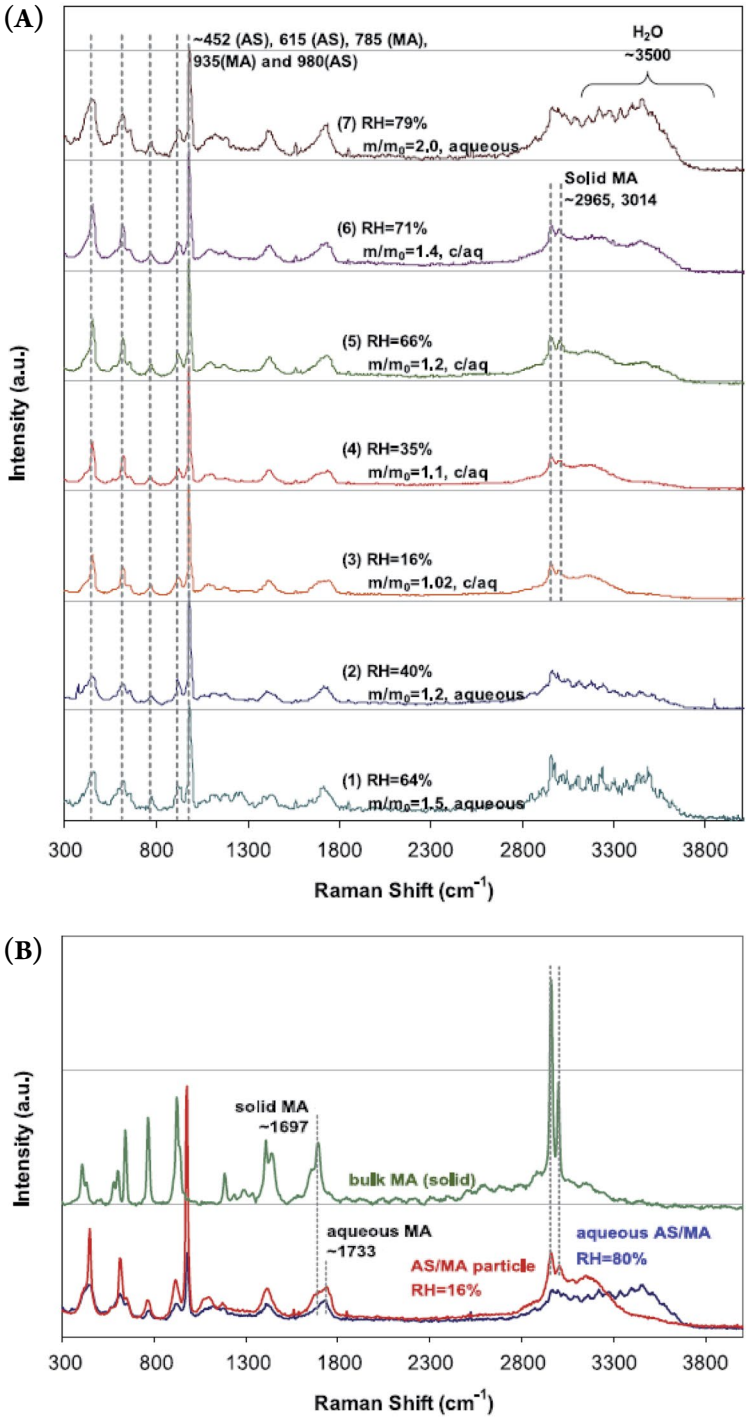

Fig. 15. (A) Raman spectra for an AS/MA particle undergoing a hygroscopic cycle. Spectra labeled "c/aq" refer to solid crystal containing aqueous droplets. (B) Comparison of the Raman spectra of a single AS/MA mixture particle at 16% and 80% RH with bulk MA crystals. Reprinted with permission from Ling, T.Y., Chan, C.K., J. Geophys. Res., 113, D14205, 2008. Copyright 2008 American Geophysical Union.

and the heterogeneous reaction of N_2O_5 on SiO_2 surface were found to be enhanced by increasing RH (Tang *et al.*, 2014).

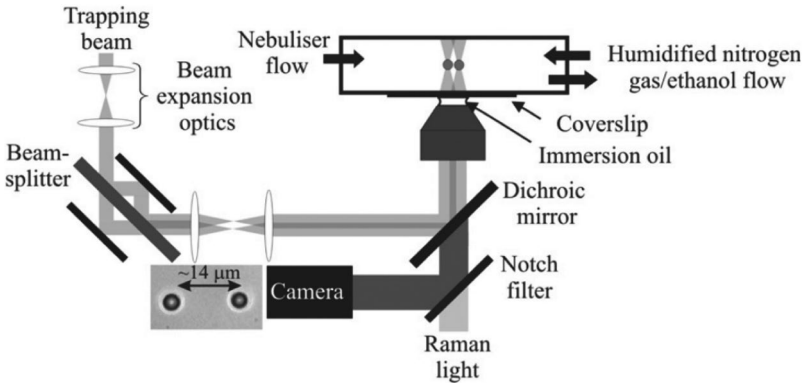

Fig. 16. The dual trapping optical tweezer system. Reprinted with permission from Mitchem, L., Hopkins, R.J., Buajarern, J., Ward, A.D., Reid, J.P., Chem. Phys. Lett., 432(2006), 362–366. Copyright 2006 Elsevier B.V. All rights reserved.

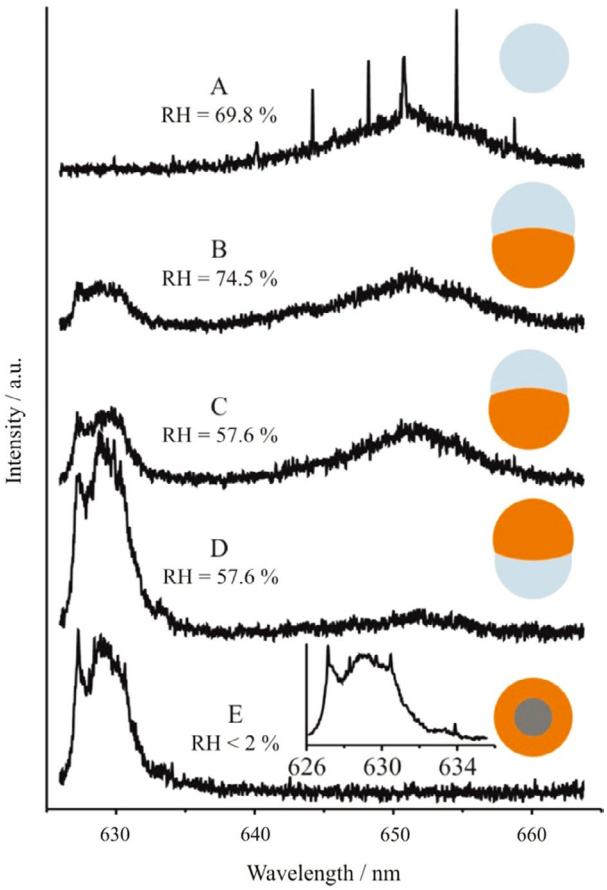

Fig. 17. Cavity enhanced Raman spectroscopy (CERS) spectra for a trapped NaCl droplet before (spectrum A) and after (spectra B–E) mixing with oleic acid at several different RHs. For each spectrum, a predicted 2-d morphology is given. Different colors represent different phases: blue, aqueous phase; orange, organic phase; gray, solid NaCl. The spectra are offset for clarity. Reprinted with permission from Dennis-Smither, B.J., Hanford, K.L., Kwamena, N.O., Miles, R.E., Reid, J.P., J. Phys. Chem. A 2012, 116, 6159–6168. Copyright 2012 American Chemical Society.

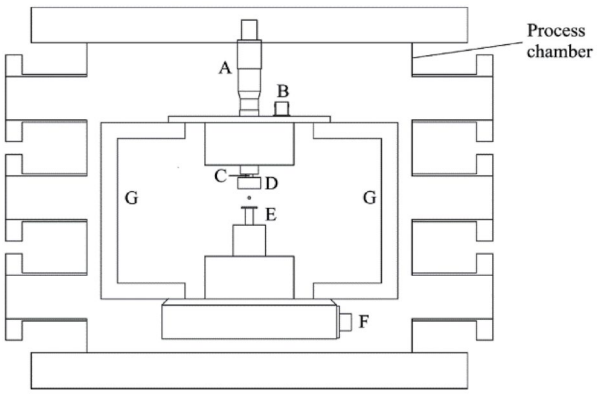

Fig. 18. Schematic diagram of an acoustic levitator (A: micrometer; B: connector; C: piezoelectric sensor; D: concave reflector; E: piezoelectric transducer). Reprinted with permission from Brotton, S.J., Kaiser, R.I., J. Phys. Chem. Lett. 2013, 4, 669–673. Copyright 2013 American Chemical Society.

3.3.3 Acoustic Levitation

Particles, larger than 20 μm, can be trapped in the acoustic levitator due to the standing sound wave generated and reflected by properly positioned piezoelectric transducer and concave reflector, respectively, as shown in Fig. 18 (Brotton and Kaiser, 2013). Acoustic levitation technique coupled with optical microscope or spectroscopy has been employed to monitor the hygroscopic behavior (Seng *et al.*, 2018; Brotton and Kaiser, 2013; Schenk *et al.*, 2012). Imidazolium-based ionic liquids with two types of anions such as fluorinated (BF_4^- and PF_6^-) and alkylsulfate anions were investigated using acoustically levitated droplets and Raman spectral analysis indicated that the ionic droplets with sulfate anions took up much more water than those with fluorinated

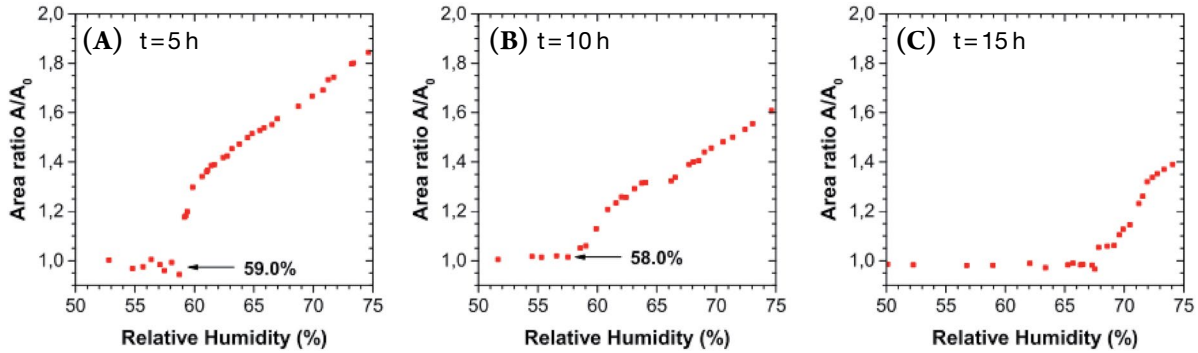

Fig. 19. Typical hygroscopic growth curves of a levitated $NaNO_3$ particle, after irradiation times of (A) 5 h, (B) 10 h and (C) 15 h. Reprinted with permission from Seng, S., Guo, F., Tobon, Y.A., Ishikawa, T., Moreau, M., Ishizaka, S., Sobanska, S., Atmos. Environ. 183(2018), 33–39. Copyright 2018 Elsevier Ltd. All rights reserved.

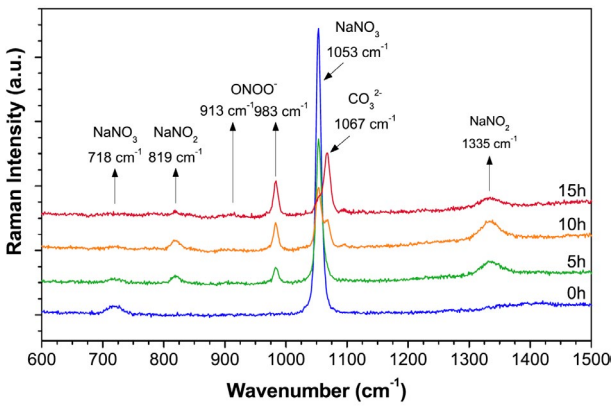

Fig. 20. Raman spectra of a levitated $NaNO_3$ droplet before and after 5 h, 10 h and 15 h of irradiation with UV-light ($\lambda = 254 \pm 25$ nm). Reprinted with permission from Seng, S., Guo, F., Tobon, Y. A., Ishikawa, T., Moreau, M., Ishizaka, S., Sobanska, S., Atmos. Environ. 183(2018), 33–39. Copyright 2018 Elsevier Ltd. All rights reserved.

anions (Schenk *et al.*, 2012). The hygroscopic properties of single, ultraviolet-irradiated $NaNO_3$ droplets in an acoustic levitator coupled with RMS were examined and the irradiation significantly affected their hygroscopic behavior of $NaNO_3$ particles (Seng *et al.*, 2018). As shown in Fig. 19, the photochemical aging processes modified the hygroscopic behavior of the $NaNO_3$ particles (Seng *et al.*, 2018). The production of NO_2^- decreased the DRH values. For long irradiation times (>5 h), these values were even more affected, which is due to the additional production of peroxynitrite and carbonate ions in individual droplets as distinguished by Raman spectra shown in Fig. 20 (Seng *et al.*, 2018). The $NaNO_3$-$NaNO_2$ deliquescence phase diagram cannot explain the hygroscopic behavior of long-term irradiated particles and the influence of CO_2 on the photo-transformation process in $NaNO_3$ droplets was claimed (Seng *et al.*, 2018).

4. SUMMARY

The ability of aerosol particles to uptake water in the air depends on their hygroscopicity, which is one of the most important physicochemical properties (Tang *et al.*, 2019; Freedman, 2017). Therefore, studies on the hygroscopicity of aerosol particles are important to comprehensively understand and predict their behavior when interacting with water vapor and further their impacts on the heterogeneous chemical reactions, atmospheric environment, and human health. The inhalable aerosol particles can typically transport and deposit in the respiratory tract of human bodies, during which the hygroscopicity of particles can influence the deposition fraction due to either growth or shrinkage of the particles as they experience the RH change when passing through the warm humid respiratory tract (Xi *et al.*, 2013). Atmospheric particles are intrinsically internal or external mixtures with inorganic and organic species and their chemical mixing state is of vital importance to understand their complex physicochemical properties, which motivates the necessity to illustrate the aerosol particles individually (Ault and Axson, 2017). In addition, microscopic and spectroscopic techniques enable the studies of physical properties and chemical compositions within homogeneous and heterogeneous individual particles. The results and data presented in this review show that the

hygroscopic measurements of atmospherically relevant aerosol particles are essential and can be achieved by a range of microscopic and spectroscopic techniques on a single particle level.

Visual observation on changes in particle size at different RHs by microscopic techniques can be used to determine hygroscopic growth factors and phase transitions. OM provides important information on the intuitive 2-D morphological evolution of pure and mixed aerosol particles on an image field as a function of RH typically for the particles with size of larger than 1 μm. AFM expands the analysis of the hygroscopicity of particles to a 3-D imaging including area and height information and even to a submicron, ultrafine level with its high spatial resolution although only one particle can be analyzed at a time. Both OM and AFM techniques are limited because they cannot provide chemical information, so that the off-line measurements by other techniques are generally used to investigate the chemical species under certain RH conditions. ESEM and ETEM equipped with EDX are powerful analytical tools as they can provide information on hygroscopic behavior, elemental compositions, mixing states, and morphology of individual particles. However, the high energy electrons used to probe the particles tend to destroy beam sensitive particles such as organics and ammonium nitrate and sulfate. STXM/NEXAFS technique is promising as it can provide chemical imaging on a spatial resolution of 40 nm and determine local chemical environments within single submicron particles, and its elemental maps allow the heterogeneous distribution of elements to be illustrated during hygroscopic measurement. In addition, the soft X-rays used in the STXM/NEXAFS measurements assure the minimum damage of the particles having light elements.

Vibrational spectroscopic techniques such as Raman and FTIR spectroscopies have been widely used because their spectra of organic and inorganic compounds are quite specific, depending on their chemical functional groups, phase states, crystallinity, and neighboring environments, which guarantee a better understanding of the hygroscopic behavior of complex aerosol particles during the hygroscopic measurement. The advantage is that the chemical functional groups, water contents, molecular interactions, and physicochemical mixing state of the aerosol particles can be directly associated with the morphological changes during the hygroscopic processes at ambient pressure once the spectroscopic methods are coupled with the RH-controlled environmental cell and optical microscopic techniques, particularly for the analysis of single particles. Raman and FTIR spectroscopies are complementary to each other as it is necessary for the molecule to have a dipole moment and a polarizability changes during the vibrations for IR and Raman signals, respectively. The spectroscopic methods can distinguish species that are challenging for the X-ray analysis such as NO_3^-. The florescence emitted from some particles after being probed by a Raman laser often makes the Raman spectral analysis challenging, and many efforts have been made to minimize the influences (Ault and Axson, 2017). The size of the particles analyzed by Raman spectroscopy is generally large (>5 μm), while the recently developed SERS (surface enhanced Raman spectroscopy) and TERS (tip-enhanced Raman spectroscopy) have extended the analysis to particles in the more atmospherically relevant size fraction (around 1 μm) (Tirella *et al.*, 2018; Fu *et al.*, 2017; Gen and Chan, 2017; Ofner *et al.*, 2016; Craig *et al.*, 2015).

Most of the techniques mentioned above are based on the investigation of substrate-deposited particles, which may have some substrate influences such as a facilitated heterogeneous nucleation, which can be eliminated in the levitation systems due to the substrate-free and contactless situation, even though the individual trapping particles are generally supermicron ones and only one particle can be measured in each experiment. One strength of the levitation systems is their ability to measure highly supersaturated droplets. The evolution of size, mass, chemical functional groups, and phase states during hygroscopic measurements of the levitated particles can be captured when the levitation systems are coupled with imaging and spectroscopic tools.

The future directions and expansions of the techniques for better elucidating hygroscopicity of aerosol particles have been well summarized and discussed in previous reviews (Tang *et al.*, 2019; Ault and Axson, 2017), and the readers are directed to those literatures. Briefly, the availability of on-line, field-portable methods, the accurate employments of RH, temperature, and pressure range, and the commerciality of the techniques would help better predict the aerosol effects on climate change and human health.

ACKNOWLEDGEMENT

This study was supported by Basic Science Research

Programs through the National Research Foundation of Korea (NRF) funded by the Ministry of Education, Science, and Technology (NRF-2018R1A2A1A05023254) and by the National Strategic Project-Fine particle of the National Research Foundation of Korea (NRF) funded by the Ministry of Science and ICT (MSIT), the Ministry of Environment (ME), and the Ministry of Health and Welfare (MOHW) (2017M3D8A1090654).

REFERENCES

Adachi, K., Freney, E.J., Buseck, P.R. (2011) Shapes of internally mixed hygroscopic aerosol particles after deliquescence, and their effect on light scattering. Geophysical Research Letters, 38, L13804. https://doi.org/10.1029/2011GL047540

Ahn, K.-H., Kim, S.-M., Jung, H.-J., Lee, M.-J., Eom, H.-J., Maskey, S., Ro, C.-U. (2010) Combined use of optical and electron microscopic techniques for the measurement of hygroscopic property, chemical composition, and morphology of individual aerosol particles. Analytical Chemistry, 82(19), 7999–8009. https://doi.org/10.1021/ac101432y

Ansari, A.S., Pandis, S.N. (1999) Prediction of multicomponent inorganic atmospheric aerosol behavior. Atmospheric Environment, 33(5), 745–757. https://doi.org/10.1016/S1352-2310(98)00221-0

Ashkin, A. (2000) History of optical trapping and manipulation of small-neutral particle, atoms, and molecules. IEEE Journal of Selected Topics in Quantum Electronics, 6(6), 841–856. http://doi.org/10.1109/2944.902132

Ault, A.P., Guasco, T.L., Ryder, O.S., Baltrusaitis, J., Cuadra-Rodriguez, L.A., Collins, D.B., Ruppel, M.J., Bertram, T.H., Prather, K.A., Grassian, V.H. (2013a) Inside versus outside: Ion redistribution in nitric acid reacted sea spray aerosol particles as determined by single particle analysis. Journal of the American Chemical Society, 135(39), 14528–14531. https://doi.org/10.1021/ja407117x

Ault, A.P., Zhao, D., Ebben, C.J., Tauber, M.J., Geiger, F.M., Prather, K.A., Grassian, V.H. (2013b) Raman microspectroscopy and vibrational sum frequency generation spectroscopy as probes of the bulk and surface compositions of size-resolved sea spray aerosol particles. Physical Chemistry Chemical Physics, 15(17), 6206–6214. https://doi.org/10.1039/c3cp43899f

Ault, A.P., Axson, J.L. (2017) Atmospheric Aerosol Chemistry: Spectroscopic and Microscopic Advances. Analytical Chemistry, 89(1), 430–452. https://doi.org/10.1021/acs.analchem.6b04670

Baustian, K., Wise, M., Tolbert, M. (2010) Depositional ice nucleation on solid ammonium sulfate and glutaric acid particles. Atmospheric Chemistry and Physics, 10(5), 2307–2317. https://doi.org/10.5194/acp-10-2307-2010

Baustian, K.J., Cziczo, D.J., Wise, M.E., Pratt, K.A., Kulkarni, G., Hallar, A.G., Tolbert, M.A. (2012) Importance of aerosol composition, mixing state, and morphology for heterogeneous ice nucleation: A combined field and laboratory approach. Journal of Geophysical Research: Atmospheres, 117, D06217. https://doi.org/10.1029/2011JD016784

Beardsley, R., Jang, M., Ori, B., Im, Y., Delcomyn, C.A., Witherspoon, N. (2013) Role of sea salt aerosols in the formation of aromatic secondary organic aerosol: yields and hygroscopic properties. Environmental Chemistry, 10(3), 167–177. https://doi.org/10.1071/EN13016

Braban, C.F., Abbatt, J.P.D., Cziczo, D.J. (2001) Deliquescence of ammonium sulfate particles at sub-eutectic temperatures. Geophysical Research Letters, 28(20), 3879–3882. https://doi.org/10.1029/2001GL013175

Brotton, S.J., Kaiser, R.I. (2013) In Situ Raman Spectroscopic Study of Gypsum ($CaSO_4 \cdot 2H_2O$) and Epsomite ($MgSO_4 \cdot 7H_2O$) Dehydration Utilizing an Ultrasonic Levitator. The Journal of Physical Chemistry Letters, 4(4), 669–673. https://doi.org/10.1021/jz301861a

Bruzewicz, D.A., Checco, A., Ocko, B.M., Lewis, E.R., McGraw, R.L., Schwartz, S.E. (2011) Reversible uptake of water on NaCl nanoparticles at relative humidity below deliquescence point observed by noncontact environmental atomic force microscopy. The Journal of Chemical Physics, 134, 044702. https://doi.org/10.1063/1.3524195

Buajarern, J., Mitchem, L., Reid, J.P. (2007) Characterizing the formation of organic layers on the surface of inorganic/aqueous aerosols by Raman spectroscopy. The Journal of Physical Chemistry A, 111(46), 11852–11859. https://doi.org/10.1021/jp075021v

Choi, M.Y., Chan, C.K., Zhang, Y.-H. (2004) Application of fluorescence spectroscopy to study the state of water in aerosols. The Journal of Physical Chemistry A, 108(7), 1133–1138. https://doi.org/10.1021/jp0355049

Choi, M.Y., Chan, C.K. (2005) Investigation of efflorescence of inorganic aerosols using fluorescence spectroscopy. The Journal of Physical Chemistry A, 109(6), 1042–1048. https://doi.org/10.1021/jp048103h

Ciobanu, V.G., Marcolli, C., Krieger, U.K., Weers, U., Peter, T. (2009) Liquid-liquid phase separation in mixed organic/inorganic aerosol particles. The Journal of Physical Chemistry A, 113(41), 10966–10978. https://doi.org/10.1021/jp905054d

Clegg, S.L., Brimblecombe, P., Wexler, A.S. (1998) Thermodynamic model of the system H^+-NH_4^+-SO_4^{2-}-NO_3^--H_2O at tropospheric temperatures. The Journal of Physical Chemistry A, 102(12), 2137–2154. https://doi.org/10.1021/jp973042r

Cohen, M.D., Flagan, R.C., Seinfeld, J.H. (1987a) Studies of concentrated electrolyte solutions using the electrodynamic balance. 1. Water activities for single-electrolyte solutions. Journal of Physical Chemistry, 91(17), 4563–4574. https://doi.org/10.1021/j100301a029

Cohen, M.D., Flagan, R.C., Seinfeld, J.H. (1987b) Studies of concentrated electrolyte solutions using the electrodynamic balance. 3. Solute nucleation. Journal of Physical Chemistry, 91(17), 4583–4590. https://doi.org/10.1021/j100301a031

Cohen, M.D., Flagan, R.C., Seinfeld, J.H. (1987c) Studies of concentrated electrolyte solutions using the electrodynamic

balance. 2. Water activities for mixed-electrolyte solutions. Journal of Physical Chemistry, 91(17), 4575–4582. https://doi.org/10.1021/j100301a030

Craig, R.L., Bondy, A.L., Ault, A.P. (2015) Surface enhanced raman spectroscopy enables observations of previously undetectable secondary organic aerosol components at the individual particle level. Analytical Chemistry, 87(15), 7510–7514. https://doi.org/10.1021/acs.analchem.5b01507

Cziczo, D., Abbatt, J. (2000) Infrared observations of the response of NaCl, $MgCl_2$, NH_4HSO_4, and NH_4NO_3 aerosols to changes in relative humidity from 298 to 238 K. The Journal of Physical Chemistry A, 104(10), 2038–2047. https://doi.org/10.1021/jp9931408

Cziczo, D.J., Nowak, J.B., Hu, J.H., Abbatt, J.P.D. (1997) Infrared spectroscopy of model tropospheric aerosols as a function of relative humidity: Observation of deliquescence and crystallization. Journal of Geophysical Research: Atmospheres, 102(D15), 18843–18850. https://doi.org/10.1029/97jd01361

Dai, Q., Hu, J., Salmeron, M. (1997) Adsorption of water on NaCl (100) surfaces: Role of atomic steps. The Journal of Physical Chemistry B, 101(11), 1994–1998. https://doi.org/10.1021/jp9625772

Davis, E.J. (1997) A History of Single Aerosol Particle Levitation. Aerosol Science and Technology, 26(3), 212–254. https://doi.org/10.1080/02786829708965426

Davis, R.D., Lance, S., Gordon, J.A., Tolbert, M.A. (2015a) Long working-distance optical trap for in situ analysis of contact-induced phase transformations. Analytical Chemistry, 87(12), 6186–6194. https://doi.org/10.1021/acs.analchem.5b00809

Davis, R.D., Lance, S., Gordon, J.A., Ushijima, S.B., Tolbert, M.A. (2015b) Contact efflorescence as a pathway for crystallization of atmospherically relevant particles. Proceedings of the National Academy of Sciences of the United States of America, 112(52), 15815–15820. https://doi.org/10.1073/pnas.1522860113

Dazzi, A., Prater, C.B., Hu, Q., Chase, D.B., Rabolt, J.F., Marcott, C. (2012) AFM-IR: combining atomic force microscopy and infrared spectroscopy for nanoscale chemical characterization. Applied Spectroscopy, 66(12), 1365–1384. https://doi.org/10.1366/12-06804

Dazzi, A., Prater, C.B. (2017) AFM-IR: Technology and applications in nanoscale infrared spectroscopy and chemical imaging. Chemical Reviews, 117(7), 5146–5173. https://doi.org/10.1021/acs.chemrev.6b00448

de Smit, E., Swart, I., Creemer, J.F., Hoveling, G.H., Gilles, M.K., Tyliszczak, T., Kooyman, P.J., Zandbergen, H.W., Morin, C., Weckhuysen, B.M., de Groot, F.M. (2008) Nanoscale chemical imaging of a working catalyst by scanning transmission X-ray microscopy. Nature, 456(7219), 222–225. https://doi.org/10.1038/nature07516

Dennis-Smither, B.J., Hanford, K.L., Kwamena, N.O., Miles, R.E., Reid, J.P. (2012) Phase, morphology, and hygroscopicity of mixed oleic acid/sodium chloride/water aerosol particles before and after ozonolysis. The Journal of Physical Chemistry A, 116(24), 6159–6168. https://doi.org/10.1021/jp211429f

Dougle, P.G., Veefkind, J.P., ten Brink, H.M. (1998) Crystallisation of mixtures of ammonium nitrate, ammonium sulphate and soot. Journal of Aerosol Science, 29(3), 375–386. https://doi.org/10.1016/S0021-8502(97)10003-9

Ebert, M., Inerle-Hof, M., Weinbruch, S. (2002) Environmental scanning electron microscopy as a new technique to determine the hygroscopic behaviour of individual aerosol particles. Atmospheric Environment, 36(39–40), 5909–5916. https://doi.org/10.1016/S1352-2310(02)00774-4

Eom, H.J., Gupta, D., Li, X., Jung, H.J., Kim, H., Ro, C.U. (2014) Influence of collecting substrates on the characterization of hygroscopic properties of inorganic aerosol particles. Analytical Chemistry, 86(5), 2648–2656. https://doi.org/10.1021/ac4042075

Freedman, M.A., Baustian, K.J., Wise, M.E., Tolbert, M.A. (2010) Characterizing the morphology of organic aerosols at ambient temperature and pressure. Analytical Chemistry, 82(19), 7965–7972. https://doi.org/10.1021/ac101437w

Freedman, M.A. (2017) Phase separation in organic aerosol. Chemical Society Reviews, 46, 7694–7705. https://doi.org/10.1039/c6cs00783j

Freney, E.J., Martin, S.T., Buseck, P.R. (2009) Deliquescence and Efflorescence of Potassium Salts Relevant to Biomass-Burning Aerosol Particles. Aerosol Science and Technology, 43(8), 799–807. https://doi.org/10.1080/02786820902946620

Freney, E.J., Adachi, K., Buseck, P.R. (2010) Internally mixed atmospheric aerosol particles: Hygroscopic growth and light scattering. Journal of Geophysical Research, 115, D19210. https://doi.org/10.1029/2009jd013558

Fu, Y., Kuppe, C., Valev, V.K., Fu, H., Zhang, L., Chen, J. (2017) Surface-enhanced raman spectroscopy: a facile and rapid method for the chemical component study of individual atmospheric aerosol. Environmental Science & Technology, 51(11), 6260–6267. https://doi.org/10.1021/acs.est.6b05910

Gao, X., Zhang, Y., Liu, Y. (2018) Temperature-dependent hygroscopic behaviors of atmospherically relevant water-soluble carboxylic acid salts studied by ATR-FTIR spectroscopy. Atmospheric Environment, 191, 312–319. https://doi.org/10.1016/j.atmosenv.2018.08.021

Ge, Z., Wexler, A.S., Johnston, M.V. (1996) Multicomponent aerosol crystallization. Journal of Colloid and Interface Science, 183(1), 68–77. https://doi.org/10.1006/jcis.1996.0519

Ge, Z., Wexler, A.S., Johnston, M.V. (1998) Deliquescence behavior of multicomponent aerosols. The Journal of Physical Chemistry A, 102(1), 173–180. https://doi.org/10.1021/jp972396f

Gen, M., Chan, C.K. (2017) Electrospray surface-enhanced Raman spectroscopy (ES-SERS) for probing surface chemical compositions of atmospherically relevant particles. Atmospheric Chemistry and Physics, 17(22), 14025-14037. https://doi.org/10.5194/acp-17-14025-2017

Ghorai, S., Laskin, A., Tivanski, A.V. (2011) Spectroscopic evidence of keto-enol tautomerism in deliquesced malonic acid particles. The Journal of Physical Chemistry A, 115(17),

4373–4380. https://doi.org/10.1021/jp112360x
Ghorai, S., Wang, B., Tivanski, A., Laskin, A. (2014) Hygroscopic properties of internally mixed particles composed of NaCl and water-soluble organic acids. Environmental Science & Technology, 48(4), 2234–2241. https://doi.org/10.1021/es404727u
Gibson, E.R., Hudson, P.K., Grassian, V.H. (2006) Physicochemical properties of nitrate aerosols: Implications for the atmosphere. The Journal of Physical Chemistry A, 110(42), 11785–11799. https://doi.org/10.1021/jp063821k
Gong, Z., Pan, Y.-L., Videen, G., Wang, C. (2018) Optical trapping and manipulation of single particles in air: Principles, technical details, and applications. Journal of Quantitative Spectroscopy and Radiative Transfer, 214, 94–119. https://doi.org/10.1016/j.jqsrt.2018.04.027
Goodman, A., Bernard, E., Grassian, V. (2001) Spectroscopic study of nitric acid and water adsorption on oxide particles: Enhanced nitric acid uptake kinetics in the presence of adsorbed water. The Journal of Physical Chemistry A, 105(26), 6443–6457. https://doi.org/10.1021/jp003722l
Griffiths, P.T., Borlace, J.S., Gallimore, P.J., Kalberer, M., Herzog, M., Pope, F.D. (2012) Hygroscopic growth and cloud activation of pollen: a laboratory and modelling study. Atmospheric Science Letters, 13(4), 289–295. https://doi.org/10.1002/asl.397
Gupta, D., Eom, H.J., Cho, H.R., Ro, C.U. (2015a) Hygroscopic behavior of NaCl-$MgCl_2$ mixture particles as nascent sea-spray aerosol surrogates and observation of efflorescence during humidification. Atmospheric Chemistry and Physics, 15(19), 11273–11290. https://doi.org/10.5194/acp-15-11273-2015
Gupta, D., Kim, H., Park, G., Li, X., Eom, H.J., Ro, C.U. (2015b) Hygroscopic properties of NaCl and $NaNO_3$ mixture particles as reacted inorganic sea-salt aerosol surrogates. Atmospheric Chemistry and Physics, 15(6), 3379–3393. https://doi.org/10.5194/acp-15-3379-2015
Gysel, M., Weingartner, E., Baltensperger, U. (2002) Hygroscopicity of aerosol particles at low temperatures. 2. Theoretical and experimental hygroscopic properties of laboratory generated aerosols. Environmental Science & Technology, 36(1), 63–68. https://doi.org/10.1021/es010055g
Haddrell, A.E., Davies, J.F., Yabushita, A., Reid, J.P. (2012) Accounting for changes in particle charge, dry mass and composition occurring during studies of single levitated particles. The Journal of Physical Chemistry A, 116(40), 9941–9953. https://doi.org/10.1021/jp304920x
Hargreaves, G., Kwamena, N.-O., Zhang, Y., Butler, J., Rushworth, S., Clegg, S., Reid, J. (2010) Measurements of the equilibrium size of supersaturated aqueous sodium chloride droplets at low relative humidity using aerosol optical tweezers and an electrodynamic balance. The Journal of Physical Chemistry A, 114(4), 1806–1815. https://doi.org/10.1021/jp9095985
Herich, H., Kammermann, L., Gysel, M., Weingartner, E., Baltensperger, U., Lohmann, U., Cziczo, D.J. (2008) In situ determination of atmospheric aerosol composition as a function of hygroscopic growth. Journal of Geophysical Research: Atmospheres, 113, D16213. https://doi.org/10.1029/2008JD009954
Herich, H., Kammermann, L., Friedman, B., Gross, D.S., Weingartner, E., Lohmann, U., Spichtinger, P., Gysel, M., Baltensperger, U., Cziczo, D.J. (2009) Subarctic atmospheric aerosol composition: 2. Hygroscopic growth properties. Journal of Geophysical Research: Atmospheres, 114(D13204). https://doi.org/10.1029/2008JD011574
Hiranuma, N., Brooks, S.D., Auvermann, B.W., Littleton, R. (2008) Using environmental scanning electron microscopy to determine the hygroscopic properties of agricultural aerosols. Atmospheric Environment, 42(9), 1983–1994. https://doi.org/10.1016/j.atmosenv.2007.12.003
Hoffman, R.C., Laskin, A., Finlayson-Pitts, B.J. (2004) Sodium nitrate particles: physical and chemical properties during hydration and dehydration, and implications for aged sea salt aerosols. Journal of Aerosol Science, 35(7), 869–887. https://doi.org/10.1016/j.jaerosci.2004.02.003
Hsu, W.-C. (1998) A novel method to measure aerosol water mass. Journal of Aerosol Science, 29(7), 827–837. https://doi.org/10.1016/S0021-8502(97)00434-5
Ibrahim, S., Romanias, M.N., Alleman, L.Y., Zeineddine, M.N., Angeli, G.K., Trikalitis, P.N., Thevenet, F. (2018) Water interaction with mineral dust aerosol: particle size and hygroscopic properties of dust. ACS Earth and Space Chemistry, 2(4), 376–386. https://doi.org/10.1021/acsearthspacechem.7b00152
Inerle-Hof, M., Weinbruch, S., Ebert, M., Thomassen, Y. (2007) The hygroscopic behaviour of individual aerosol particles in nickel refineries as investigated by environmental scanning electron microscopy. Journal of Environmental Monitoring, 9, 301–306. https://doi.org/10.1039/B618252F
Jing, B., Tong, S., Liu, Q., Li, K., Wang, W., Zhang, Y., Ge, M. (2016) Hygroscopic behavior of multicomponent organic aerosols and their internal mixtures with ammonium sulfate, Atmospheric Chemistry and Physics, 16(6), 4101–4118. https://doi.org/10.5194/acp-16-4101-2016
Jordanov, N., Zellner, R. (2006) Investigations of the hygroscopic properties of ammonium sulfate and mixed ammonium sulfate and glutaric acid micro droplets by means of optical levitation and Raman spectroscopy. Physical Chemistry Chemical Physics, 8(23), 2759–2764. https://doi.org/10.1039/B604439E
Joshi, N., Romanias, M.N., Riffault, V., Thevenet, F. (2017) Investigating water adsorption onto natural mineral dust particles: Linking DRIFTS experiments and BET theory. Aeolian Research, 27, 35–45. https://doi.org/10.1016/j.aeolia.2017.06.001
Kelly, J.T. (2005) Thermodynamics of carbonates and hydrates related to heterogeneous reactions involving mineral aerosol. Journal of Geophysical Research, 110, D11201. https://doi.org/10.1029/2004jd005583
Kelly, S.T., Nigge, P., Prakash, S., Laskin, A., Wang, B., Tyliszczak, T., Leone, S.R., Gilles, M.K. (2013) An environmental sample chamber for reliable scanning transmission x-ray microscopy measurements under water vapor. Review of Scientific Instruments, 84, 073708. https://doi.org/10.1063/1.4816649
Kim, H., Lee, M.-J., Jung, H.-J., Eom, H.-J., Maskey, S., Ahn,

K.-H., Ro, C.-U. (2012) Hygroscopic behavior of wet dispersed and dry deposited $NaNO_3$ particles, Atmospheric Environment, 60, 68–75. https://doi.org/10.1016/j.atmosenv.2012.06.011

Kreidenweis, S., Asa-Awuku, A. (2014) Aerosol Hygroscopicity: Particle water content and its role in atmospheric processes. Treatise on Geochemistry (Second Edition), 5, 331–361. https://doi.org/10.1016/B978-0-08-095975-7.00418-6

Krieger, U.K., Marcolli, C., Reid, J.P. (2012) Exploring the complexity of aerosol particle properties and processes using single particle techniques. Chemical Society Reviews, 41(19), 6631–6662. https://doi.org/10.1039/c2cs35082c

Krueger, B.J. (2003) The transformation of solid atmospheric particles into liquid droplets through heterogeneous chemistry: Laboratory insights into the processing of calcium containing mineral dust aerosol in the troposphere. Geophysical Research Letters, 30(3). https://doi.org/10.1029/2002gl016563

Krueger, B.J., Grassian, V.H., Cowin, J.P., Laskin, A. (2004) Heterogeneous chemistry of individual mineral dust particles from different dust source regions: the importance of particle mineralogy. Atmospheric Environment, 38(36), 6253–6261. https://doi.org/10.1016/j.atmosenv.2004.07.010

Laskin, A., Iedema, M.J., Ichkovich, A., Graber, E.R., Taraniuk, I., Rudich, Y. (2005) Direct observation of completely processed calcium carbonate dust particles. Faraday Discussions, 130, 453–468. https://doi.org/10.1039/b417366j

Laskin, A., Moffet, R.C., Gilles, M.K., Fast, J.D., Zaveri, R.A., Wang, B., Nigge, P., Shutthanandan, J. (2012) Tropospheric chemistry of internally mixed sea salt and organic particles: Surprising reactivity of NaCl with weak organic acids. Journal of Geophysical Research: Atmospheres, 117, D15302. https://doi.org/10.1029/2012jd017743

Laskina, O., Morris, H.S., Grandquist, J.R., Estillore, A.D., Stone, E.A., Grassian, V.H., Tivanski, A.V. (2015a) Substrate-deposited sea spray aerosol particles: Influence of analytical method, substrate, and storage conditions on particle size, phase, and morphology. Environmental Science & Technology, 49(22), 13447–13453. https://doi.org/10.1021/acs.est.5b02732

Laskina, O., Morris, H.S., Grandquist, J.R., Qin, Z., Stone, E.A., Tivanski, A.V., Grassian, V.H. (2015b) Size matters in the water uptake and hygroscopic growth of atmospherically relevant multicomponent aerosol particles. The Journal of Physical Chemistry A, 119(19), 4489–4497. https://doi.org/10.1021/jp510268p

Lee, A.K., Ling, T.Y., Chan, C.K. (2008) Understanding hygroscopic growth and phase transformation of aerosols using single particle Raman spectroscopy in an electrodynamic balance. Faraday Discussions, 137, 245–263; discussion 297–318. https://doi.org/10.1039/b704580h

Lee, C.-T., Hsu, W.-C. (2000) The measurement of liquid water mass associated with collected hygroscopic particles. Journal of Aerosol Science, 31(2), 189–197. https://doi.org/10.1016/S0021-8502(99)00048-8

Lee, C.-T., Chang, S.-Y. (2002) A GC-TCD method for measuring the liquid water mass of collected aerosols. Atmospheric Environment, 36(11), 1883–1894. https://doi.org/10.1016/S1352-2310(02)00088-2

Lehmpuhl, D.W., Ramirez-Aguilar, K.A., Michel, A.E., Rowlen, K.L., Birks, J.W. (1999) Physical and chemical characterization of atmospheric aerosols by atomic force microscopy. Analytical Chemistry, 71(2), 379–383. https://doi.org/10.1021/ac980849m

Li, W., Chi, J., Shi, Z., Wang, X., Chen, B., Wang, Y., Li, T., Chen, J., Zhang, D., Wang, Z., Shi, C., Liu, L., Wang, W. (2014a) Composition and hygroscopicity of aerosol particles at Mt. Lu in South China: Implications for acid precipitation. Atmospheric Environment, 94, 626–636. https://doi.org/10.1016/j.atmosenv.2014.06.003

Li, W., Shao, L., Shi, Z., Chen, J., Yang, L., Yuan, Q., Yan, C., Zhang, X., Wang, Y., Sun, J., Zhang, Y., Shen, X., Wang, Z., Wang, W. (2014b) Mixing state and hygroscopicity of dust and haze particles before leaving Asian continent. Journal of Geophysical Research: Atmospheres, 119(2), 1044–1059. https://doi.org/10.1002/2013jd021003

Li, W., Shao, L., Zhang, D., Ro, C.-U., Hu, M., Bi, X., Geng, H., Matsuki, A., Niu, H., Chen, J. (2016) A review of single aerosol particle studies in the atmosphere of East Asia: morphology, mixing state, source, and heterogeneous reactions. Journal of Cleaner Production, 112(2), 1330–1349. https://doi.org/10.1016/j.jclepro.2015.04.050

Li, W., Liu, L., Xu, L., Zhang, J., Yuan, Q., Ding, X., Hu, W., Fu, P., Zhang, D. (2020) Overview of primary biological aerosol particles from a Chinese boreal forest: Insight into morphology, size, and mixing state at microscopic scale. Science of The Total Environment, 719, 137520. https://doi.org/10.1016/j.scitotenv.2020.137520

Li, X.-H., Wang, F., Lu, P.-D., Dong, J.-L., Wang, L.-Y., Zhang, Y.-H. (2006) Confocal Raman observation of the efflorescence/deliquescence processes of individual $NaNO_3$ particles on quartz. The Journal of Physical Chemistry B, 110(49), 24993–24998. https://doi.org/10.1021/jp064221o

Li, X., Gupta, D., Eom, H.-J., Kim, H., Ro, C.-U. (2014c) Deliquescence and efflorescence behavior of individual NaCl and KCl mixture aerosol particles. Atmospheric Environment, 82, 36–43. https://doi.org/10.1016/j.atmosenv.2013.10.011

Li, X., Gupta, D., Lee, J., Park, G., Ro, C.U. (2017) Real-time investigation of chemical compositions and hygroscopic properties of aerosols generated from NaCl and malonic acid mixture solutions using in situ Raman microspectrometry. Environmental Science and Technology, 51(1), 263–270. https://doi.org/10.1021/acs.est.6b04356

Li, X., Song, S., Zhou, W., Hao, J., Worsnop, D.R., Jiang, J. (2019) Interactions between aerosol organic components and liquid water content during haze episodes in Beijing. Atmospheric Chemistry and Physics, 19(19), 12163–12174. https://doi.org/10.5194/acp-19-12163-2019

Lightstone, J.M., Onasch, T.B., Imre, D., Oatis, S. (2000) Deliquescence, efflorescence, and water activity in ammonium nitrate and mixed ammonium nitrate/succinic acid microparticles. The Journal of Physical Chemistry A, 104(41), 9337–9346. https://doi.org/10.1021/jp002137h

Ling, T.Y., Chan, C.K. (2007) Formation and transformation of metastable double salts from the crystallization of mixed ammonium nitrate and ammonium sulfate particles. Environmental Science & Technology, 41(23), 8077–8083, https://doi.org/10.1021/es071419t

Ling, T.Y., Chan, C.K. (2008) Partial crystallization and deliquescence of particles containing ammonium sulfate and dicarboxylic acids. Journal of Geophysical Research, 113, D14205. https://doi.org/10.1029/2008jd009779

Liu, Y., Cain, J.P., Wang, H., Laskin, A. (2007) Kinetic study of heterogeneous reaction of deliquesced NaCl particles with gaseous HNO_3 using particle-on-substrate stagnation flow reactor approach. The Journal of Physical Chemistry A, 111(40), 10026–10043. https://doi.org/10.1021/jp072005p

Liu, Y., Yang, Z., Desyaterik, Y., Gassman, P.L., Wang, H., Laskin, A. (2008a) Hygroscopic behavior of substrate-deposited particles studied by micro-FT-IR spectroscopy and complementary methods of particle analysis. Analytical Chemistry, 80(3), 633–642. https://doi.org/10.1021/ac701638r

Liu, Y., Zhu, T., Zhao, D., Zhang, Z. (2008b) Investigation of the hygroscopic properties of $Ca(NO_3)_2$ and internally mixed $Ca(NO_3)_2/CaCO_3$ particles by micro-Raman spectrometry. Atmospheric Chemistry and Physics, 8(23), 7205–7215. https://doi.org/10.5194/acp-8-7205-2008

Liu, Y., Laskin, A. (2009) Hygroscopic properties of CH_3SO_3Na, $CH_3SO_3NH_4$, $(CH_3SO_3)_2Mg$, and $(CH_3SO_3)_2Ca$ particles studied by micro-FTIR spectroscopy. The Journal of Physical Chemistry A, 113(8), 1531–1538. https://doi.org/10.1021/jp8079149

Lu, P.-D., Wang, F., Zhao, L.-J., Li, W.-X., Li, X.-H., Dong, J.-L., Zhang, Y.-H., Lu, G.-Q. (2008) Molecular events in deliquescence and efflorescence phase transitions of sodium nitrate particles studied by Fourier transform infrared attenuated total reflection spectroscopy. The Journal of Chemical Physics, 129, 104509. https://doi.org/10.1063/1.2973623

Ma, Q., He, H., Liu, Y. (2010) In situ DRIFTS study of hygroscopic behavior of mineral aerosol. Journal of Environmental Sciences, 22(4), 555–560. https://doi.org/10.1016/s1001-0742(09)60145-5

Ma, Q., He, H. (2012) Synergistic effect in the humidifying process of atmospheric relevant calcium nitrate, calcite and oxalic acid mixtures. Atmospheric Environment, 50, 97–102. https://doi.org/10.1016/j.atmosenv.2011.12.057

Ma, Q., Liu, Y., Liu, C., He, H. (2012) Heterogeneous reaction of acetic acid on MgO, alpha-Al_2O_3, and $CaCO_3$ and the effect on the hygroscopic behaviour of these particles. Physical Chemistry Chemical Physics, 14(23), 8403–8409. https://doi.org/10.1039/c2cp40510e

Ma, Q., Ma, J., Liu, C., Lai, C., He, H. (2013) Laboratory study on the hygroscopic behavior of external and internal C_2-C_4 dicarboxylic acid-NaCl mixtures, Environmental Science & Technology, 47(18), 10381–10388. https://doi.org/10.1021/es4023267

Maria, S.F., Russell, L.M., Gilles, M.K., Myneni, S.C. (2004) Organic aerosol growth mechanisms and their climate-forcing implications. Science, 306(5703), 1921–1924, https://doi.org/10.1126/science.1103491

Martin, S.T. (2000) Phase transitions of aqueous atmospheric particles. Chemical Reviews, 100(9), 3403–3454. https://doi.org/10.1021/cr990034t

Martin, S.T., Schlenker, J.C., Malinowski, A., Hung, H.M., Rudich, Y. (2003) Crystallization of atmospheric sulfate-nitrate-ammonium particles. Geophysical Research Letters, 30(21). https://doi.org/10.1029/2003GL017930

Matsumura, T., Hayashi, M. (2007) Hygroscopic Growth of an $(NH_4)_2SO_4$ Aqueous Solution Droplet Measured Using an Environmental Scanning Electron Microscope (ESEM). Aerosol Science and Technology, 41(8), 770–774. https://doi.org/10.1080/02786820701436831

McInnes, L., Quinn, P., Covert, D., Anderson, T. (1996) Gravimetric analysis, ionic composition, and associated water mass of the marine aerosol. Atmospheric Environment, 30(6), 869–884. https://doi.org/10.1016/1352-2310(95)00354-1

McMurry, P.H., Litchy, M., Huang, P.-F., Cai, X., Turpin, B.J., Dick, W.D., Hanson, A. (1996) Elemental composition and morphology of individual particles separated by size and hygroscopicity with the TDMA. Atmospheric Environment, 30(1), 101–108. https://doi.org/10.1016/1352-2310(95)00235-Q

Mikhailov, E., Vlasenko, S., Martin, S., Koop, T., Pöschl, U. (2009) Amorphous and crystalline aerosol particles interacting with water vapor: conceptual framework and experimental evidence for restructuring, phase transitions and kinetic limitations. Atmospheric Chemistry and Physics, 9(24), 9491–9522. https://doi.org/10.5194/acp-9-9491-2009

Mitchem, L., Buajarern, J., Hopkins, R.J., Ward, A.D., Gilham, R.J., Johnston, R.L., Reid, J.P. (2006a) Spectroscopy of growing and evaporating water droplets: exploring the variation in equilibrium droplet size with relative humidity. The Journal of Physical Chemistry A, 110(26), 8116–8125. https://doi.org/10.1021/jp061135f

Mitchem, L., Buajarern, J., Ward, A.D., Reid, J.P. (2006b) A strategy for characterizing the mixing state of immiscible aerosol components and the formation of multiphase aerosol particles through coagulation. The Journal of Physical Chemistry B, 110(28), 13700–13703. https://doi.org/10.1021/jp062874z

Mitchem, L., Hopkins, R.J., Buajarern, J., Ward, A.D., Reid, J.P. (2006c) Comparative measurements of aerosol droplet growth, Chemical Physics Letters, 432(1–3), 362–366. https://doi.org/10.1016/j.cplett.2006.10.053

Mitchem, L., Reid, J.P. (2008) Optical manipulation and characterisation of aerosol particles using a single-beam gradient force optical trap. Chemical Society Reviews, 37(4), 756–769. https://doi.org/10.1039/b609713h

Morris, H.S., Grassian, V.H., Tivanski, A.V. (2015) Humidity-dependent surface tension measurements of individual inorganic and organic submicrometre liquid particles. Chemical Science, 6(5), 3242–3247. https://doi.org/10.1039/c4sc03716b.

Morris, H.S., Estillore, A.D., Laskina, O., Grassian, V.H., Tivanski, A.V. (2016) Quantifying the Hygroscopic Growth of Individual Submicrometer Particles with Atomic Force Micros-

copy. Analytical Chemistry, 88(7), 3647–3654. https://doi.org/10.1021/acs.analchem.5b04349

Mozurkewich, M., Calvert, J.G. (1988) Reaction probability of N_2O_5 on aqueous aerosols. Journal of Geophysical Research: Atmospheres, 93(D12), 15889–15896. https://doi.org/10.1029/JD093iD12p15889

Navea, J.G., Richmond, E., Stortini, T., Greenspan, J. (2017) Water Adsorption Isotherms on Fly Ash from Several Sources. Langmuir, 33(39), 10161–10171. https://doi.org/10.1021/acs.langmuir.7b02028

Neubauer, K.R., Johnston, M.V., Wexler, A.S. (1998) Humidity effects on the mass spectra of single aerosol particles. Atmospheric Environment, 32(14), 2521–2529. https://doi.org/10.1016/S1352-2310(98)00005-3

Ofner, J., Deckert-Gaudig, T., Kamilli, K.A., Held, A., Lohninger, H., Deckert, V., Lendl, B. (2016) Tip-enhanced raman spectroscopy of atmospherically relevant aerosol nanoparticles. Analytical Chemistry, 88(19), 9766–9772. https://doi.org/10.1021/acs.analchem.6b02760

Pant, A., Fok, A., Parsons, M.T., Mak, J., Bertram, A.K. (2004) Deliquescence and crystallization of ammonium sulfate-glutaric acid and sodium chloride-glutaric acid particles. Geophysical Research Letters, 31, L12111. https://doi.org/10.1029/2004gl020025

Pant, A., Parsons, M.T., Bertram, A.K. (2006) Crystallization of aqueous ammonium sulfate particles internally mixed with soot and kaolinite: Crystallization relative humidities and nucleation rates. The Journal of Physical Chemistry A, 110(28), 8701–8709. https://doi.org/10.1021/jp060985s

Park, K., Kim, J.-S., Miller, A.L. (2009) A study on effects of size and structure on hygroscopicity of nanoparticles using a tandem differential mobility analyzer and TEM. Journal of Nanoparticle Research, 11, 175–183. https://doi.org/10.1007/s11051-008-9462-4

Parsons, M.T., Knopf, D.A., Bertram, A.K. (2004a) Deliquescence and crystallization of ammonium sulfate particles internally mixed with water-soluble organic compounds. The Journal of Physical Chemistry A, 108(52), 11600–11608. https://doi.org/10.1021/jp0462862

Parsons, M.T., Mak, J., Lipetz, S.R., Bertram, A.K. (2004b) Deliquescence of malonic, succinic, glutaric, and adipic acid particles. Journal of Geophysical Research: Atmospheres, 109, D06212. https://doi.org/10.1029/2003JD004075

Parsons, M.T., Riffell, J.L., Bertram, A.K. (2006) Crystallization of aqueous inorganic- malonic acid particles: Nucleation rates, dependence on size, and dependence on the ammonium-to-sulfate ratio. The Journal of Physical Chemistry A, 110(26), 8108–8115. https://doi.org/10.1021/jp057074n

Peng, C., Chan, C.K. (2001) The water cycles of water-soluble organic salts of atmospheric importance. Atmospheric Environment, 35(7), 1183–1192. https://doi.org/10.1016/S1352-2310(00)00426-X

Peng, C., Chan, M.N., Chan, C.K. (2001) The hygroscopic properties of dicarboxylic and multifunctional acids: Measurements and UNIFAC predictions. Environmental Science & Technology, 35(22), 4495–4501. https://doi.org/10.1021/es0107531

Piens, D.S., Kelly, S.T., Harder, T.H., Petters, M.D., O'Brien, R. E., Wang, B., Teske, K., Dowell, P., Laskin, A., Gilles, M.K. (2016) Measuring mass-based hygroscopicity of atmospheric particles through in situ imaging. Environmental Science & Technology, 50(10), 5172–5180. https://doi.org/10.1021/acs.est.6b00793

Pöhlker, C., Saturno, J., Krüger, M.L., Förster, J.-D., Weigand, M., Wiedemann, K.T., Bechtel, M., Artaxo, P., Andreae, M.O. (2014) Efflorescence upon humidification? X-ray microspectroscopic in situ observation of changes in aerosol microstructure and phase state upon hydration. Geophysical Research Letters, 41(10), 3681–3689. https://doi.org/10.1002/2014gl059409

Pope, F.D. (2010) Pollen grains are efficient cloud condensation nuclei. Environmental Research Letters, 5(4), 044015. https://doi.org/10.1088/1748-9326/5/4/044015

Pope, F.D., Dennis-Smither, B.J., Griffiths, P.T., Clegg, S.L., Cox, R.A. (2010) Studies of single aerosol particles containing malonic acid, glutaric acid, and their mixtures with sodium chloride. I. Hygroscopic growth. The Journal of Physical Chemistry A, 114(16), 5335–5341. https://doi.org/10.1021/jp100059k

Poschl, U., Shiraiwa, M. (2015) Multiphase chemistry at the atmosphere-biosphere interface influencing climate and public health in the anthropocene. Chemical Reviews, 115(10), 444074475. https://doi.org/10.1021/cr500487s

Pósfai, M., Xu, H., Anderson, J.R., Buseck, P.R. (1998) Wet and dry sizes of atmospheric aerosol particles: An AFM-TEM Study. Geophysical Research Letters, 25(11), 1907–1910. https://doi.org/10.1029/98gl01416

Pósfai, M., Simonics, R., Li, J., Hobbs, P.V., Buseck, P.R. (2003) Individual aerosol particles from biomass burning in southern Africa: 1. Compositions and size distributions of carbonaceous particles. Journal of Geophysical Research: Atmospheres, 108(D13), 8483. https://doi.org/10.1029/2002JD002291

Prather, K.A., Bertram, T.H., Grassian, V.H., Deane, G.B., Stokes, M.D., DeMott, P.J., Aluwihare, L.I., Palenik, B.P., Azam, F., Seinfeld, J.H. (2013) Bringing the ocean into the laboratory to probe the chemical complexity of sea spray aerosol. Proceedings of the National Academy of Sciences of the United States of America, 110(19), 7550–7555. https://doi.org/10.1073/pnas.1300262110

Rader, D., McMurry, P.H. (1986) Application of the tandem differential mobility analyzer to studies of droplet growth or evaporation. Journal of Aerosol Science, 17(5), 771–787. https://doi.org/10.1016/0021-8502(86)90031-5

Reid, J.P., Sayer, R.M. (2003) Heterogeneous atmospheric aerosol chemistry: laboratory studies of chemistry on water droplets, Chemical Society Reviews, 32, 70–79. https://doi.org/10.1039/b204463n

Reid, J.P., Meresman, H., Mitchem, L., Symes, R. (2007) Spectroscopic studies of the size and composition of single aerosol droplets. International Reviews in Physical Chemistry, 26(1), 139–192. https://doi.org/10.1080/01442350601081899

Rkiouak, L., Tang, M.J., Camp, J.C., McGregor, J., Watson, I.M., Cox, R.A., Kalberer, M., Ward, A.D., Pope, F.D. (2014) Optical trapping and Raman spectroscopy of solid particles.

Physical Chemistry Chemical Physics, 16(23), 11426–11434. https://doi.org/10.1039/c4cp00994k

Ro, C.-U., Hwang, H., Kim, H., Chun, Y., Van Grieken, R. (2005) Single-particle characterization of four "Asian Dust" samples collected in Korea, using low-Z particle electron probe X-ray microanalysis. Environmental Science & Technology, 39(6), 1409–1419. https://doi.org/10.1021/es049772b

Ryder, O.S., Ault, A.P., Cahill, J.F., Guasco, T.L., Riedel, T.P., Cuadra-Rodriguez, L.A., Gaston, C.J., Fitzgerald, E., Lee, C., Prather, K.A. (2014) On the role of particle inorganic mixing state in the reactive uptake of N_2O_5 to ambient aerosol particles. Environmental Science & Technology, 48(3), 1618–1627. https://doi.org/10.1021/es4042622

Saul, T.D., Tolocka, M.P., Johnston, M.V. (2006) Reactive uptake of nitric acid onto sodium chloride aerosols across a wide range of relative humidities. The Journal of Physical Chemistry A, 110(24), 7614–7620. https://doi.org/10.1021/jp060639a

Schenk, J., Panne, U., Albrecht, M. (2012) Interaction of levitated ionic liquid droplets with water, The Journal of Physical Chemistry B, 116(48), 14171–14177. https://doi.org/10.1021/jp309661p

Schlenker, J.C., Malinowski, A., Martin, S.T., Hung, H.-M., Rudich, Y. (2004) Crystals formed at 293 k by aqueous sulfate-nitrate-ammonium-proton aerosol particles. The Journal of Physical Chemistry A, 108(43), 9375–9383. https://doi.org/10.1021/jp047836z

Schuttlefield, J., Al-Hosney, H., Zachariah, A., Grassian, V.H. (2007) Attenuated total reflection Fourier transform infrared spectroscopy to investigate water uptake and phase transitions in atmospherically relevant particles. Applied Spectroscopy, 61(3), 283–292. https://doi.org/10.1366/000370207780220868

Semeniuk, T., Wise, M., Martin, S., Russell, L., Buseck, P. (2007a) Water uptake characteristics of individual atmospheric particles having coatings. Atmospheric Environment, 41(29), 6225–6235. https://doi.org/10.1016/j.atmosenv.2007.04.001

Semeniuk, T.A., Wise, M.E., Martin, S.T., Russell, L.M., Buseck, P.R. (2007b) Hygroscopic behavior of aerosol particles from biomass fires using environmental transmission electron microscopy. Journal of Atmospheric Chemistry, 56, 259–273. https://doi.org/10.1007/s10874-006-9055-5

Seng, S., Guo, F., Tobon, Y.A., Ishikawa, T., Moreau, M., Ishizaka, S., Sobanska, S. (2018) Deliquescence behavior of photo-irradiated single $NaNO_3$ droplets. Atmospheric Environment, 183, 33–39. https://doi.org/10.1016/j.atmosenv.2018.04.007

Shi, Z., Zhang, D., Hayashi, M., Ogata, H., Ji, H., Fujiie, W. (2008) Influences of sulfate and nitrate on the hygroscopic behaviour of coarse dust particles. Atmospheric Environment, 42(4), 822–827. https://doi.org/10.1016/j.atmosenv.2007.10.037

Steimer, S.S., Lampimäki, M., Coz, E., Gržinić, G., Ammann, M. (2014) The influence of physical state on shikimic acid ozonolysis: a case for in situ microspectroscopy. Atmospheric Chemistry and Physics, 14(19), 10761–10772. https://doi.org/10.5194/acp-14-10761-2014

Sun, J., Liu, L., Xu, L., Wang, Y., Wu, Z., Hu, M., Shi, Z., Li, Y., Zhang, X., Chen, J., Li, W. (2018) Key Role of Nitrate in Phase Transitions of Urban Particles: Implications of Important Reactive Surfaces for Secondary Aerosol Formation. Journal of Geophysical Research: Atmospheres, 123(2), 1234–1243. https://doi.org/10.1002/2017jd027264

Swietlicki, E., Hansson, H.-C., Hämeri, K., Svenningsson, B., Massling, A., McFiggans, G., McMurry, P.H., Petäjä, T., Tunved, P., Gysel, M. (2008) Hygroscopic properties of submicrometer atmospheric aerosol particles measured with H-TDMA instruments in various environments - a review. Tellus B: Chemical and Physical Meteorology, 60(3), 432–469. https://doi.org/10.1111/j.1600-0889.2008.00350.x

Tang, I. (1976) Phase transformation and growth of aerosol particles composed of mixed salts. Journal of Aerosol Science, 7(5), 361–371. https://doi.org/10.1016/0021-8502(76)90022-7

Tang, I. (1980) Deliquescence properties and particle size change of hygroscopic aerosols, in "Generation of aerosols and facilities for exposure experiments", edited by: K. Willeke, Chapter 7, 153–167, Ann Arbor Science, Ann Arbor, MI.

Tang, I., Munkelwitz, H. (1994) Water activities, densities, and refractive indices of aqueous sulfates and sodium nitrate droplets of atmospheric importance. Journal of Geophysical Research: Atmospheres, 99(D9), 18801–18808. https://doi.org/10.1029/94JD01345

Tang, I., Fung, K. (1997) Hydration and Raman scattering studies of levitated microparticles: $Ba(NO_3)_2$, $Sr(NO_3)_2$, and $Ca(NO_3)_2$. The Journal of Chemical Physics, 106(5), 1653–1660. https://doi.org/10.1063/1.473318

Tang, I.N., Tridico, A., Fung, K. (1997) Thermodynamic and optical properties of sea salt aerosols. Journal of Geophysical Research: Atmospheres, 102(D19), 23269–23275. https://doi.org/10.1029/97JD01806

Tang, I.N., Fung, K.H., Imre, D.G., Munkelwitz, H.R. (2007) Phase Transformation and Metastability of Hygroscopic Microparticles. Aerosol Science and Technology, 23(3), 443–453. https://doi.org/10.1080/02786829508965327

Tang, M., Cziczo, D.J., Grassian, V.H. (2016a) Interactions of Water with Mineral Dust Aerosol: Water Adsorption, Hygroscopicity, Cloud Condensation, and Ice Nucleation. Chemical Reviews, 116(7), 4205–4259. https://doi.org/10.1021/acs.chemrev.5b00529

Tang, M., Larish, W.A., Fang, Y., Gankanda, A., Grassian, V.H. (2016b) Heterogeneous Reactions of Acetic Acid with Oxide Surfaces: Effects of Mineralogy and Relative Humidity. The Journal of Physical Chemistry A, 120(28), 5609–5616. https://doi.org/10.1021/acs.jpca.6b05395

Tang, M., Chan, C.K., Li, Y.J., Su, H., Ma, Q., Wu, Z., Zhang, G., Wang, Z., Ge, M., Hu, M., He, H., Wang, X. (2019) A review of experimental techniques for aerosol hygroscopicity studies. Atmospheric Chemistry and Physics, 19(19), 12631–12686. https://doi.org/10.5194/acp-19-12631-2019

Tang, M.J., Camp, J.C., Rkiouak, L., McGregor, J., Watson, I.M., Cox, R.A., Kalberer, M., Ward, A.D., Pope, F.D. (2014) Heterogeneous interaction of SiO_2 with N_2O_5: aerosol flow tube

and single particle optical levitation-Raman spectroscopy studies. The Journal of Physical Chemistry A, 118(38), 8817–8827. https://doi.org/10.1021/jp506753c

ten Brink, H.M. (1998) Reactive uptake of HNO_3 and H_2SO_4 in sea-salt (NaCl) particles. Journal of Aerosol Science, 29(1–2), 57–64. https://doi.org/10.1016/S0021-8502(97)00460-6

Tirella, P.N., Craig, R.L., Tubbs, D.B., Olson, N.E., Lei, Z., Ault, A.P. (2018) Extending surface enhanced Raman spectroscopy (SERS) of atmospheric aerosol particles to the accumulation mode (150–800 nm). Environmental Science: Processes & Impacts, 20(11), 1570–1580. https://doi.org/10.1039/c8em00276b

Tong, H.-J., Reid, J.P., Dong, J.-L., Zhang, Y.-H. (2010) Observation of the crystallization and supersaturation of mixed component $NaNO_3$-Na_2SO_4 droplets by FTIR-ATR and Raman spectroscopy. The Journal of Physical Chemistry A, 114(46), 12237–12243. https://doi.org/10.1021/jp1080548

Tong, H.J., Ouyang, B., Nikolovski, N., Lienhard, D.M., Pope, F.D., Kalberer, M. (2015) A new electrodynamic balance (EDB) design for low-temperature studies: application to immersion freezing of pollen extract bioaerosols. Atmospheric Measurement Techniques, 8(3), 1183–1195. https://doi.org/10.5194/amt-8-1183-2015

Treuel, L., Pederzani, S., Zellner, R. (2009) Deliquescence behaviour and crystallisation of ternary ammonium sulfate/dicarboxylic acid/water aerosols. Physical Chemistry Chemical Physics, 11(36), 7976–7984. https://doi.org/10.1039/b905007h

Treuel, L., Butler, J.R., Hargreaves, G., Reid, J.P. (2010) Probing the Equilibrium Size and Hydrogen Bonding Structure in Aqueous Aerosol Droplets. Zeitschrift für Physikalische Chemie, 224(7–8), 1185–1204. https://doi.org/10.1524/zpch.2010.6147

Trunk, M., Lübben, J., Popp, J., Schrader, B., Kiefer, W. (1997) Investigation of a phase transition in a single optically levitated microdroplet by Raman-Mie scattering. Applied optics, 36(15), 3305–3309. https://doi.org/10.1364/AO.36.003305

Twomey, S. (1953) The Identification of Individual Hygroscopic Particles in the Atmosphere by a Phase-Transition Method. Journal of Applied Physics, 24(9), 1099–1102. https://doi.org/10.1063/1.1721454

Twomey, S. (1954) The composition of hygroscopic particles in the atmosphere. Journal of Meteorology, 11(4), 334–338. https://doi.org/10.1175/1520-0469(1954)011<0334:TCOHPI>2.0.CO;2

Usher, C.R., Michel, A.E., Grassian, V.H. (2003) Reactions on mineral dust. Chemical Reviews, 103(12), 4883–4940. https://doi.org/10.1021/cr020657y

Wang, B., Laskin, A. (2014) Reactions between water-soluble organic acids and nitrates in atmospheric aerosols: Recycling of nitric acid and formation of organic salts. Journal of Geophysical Research: Atmospheres, 119(6), 3335–3351. https://doi.org/10.1002/2013jd021169

Wang, F., Zhang, Y.-H., Li, S.-H., Wang, L.-Y., Zhao, L.-J. (2005) A strategy for single supersaturated droplet analysis: confocal Raman investigations on the complicated hygroscopic properties of individual $MgSO_4$ droplets on the quartz substrate. Analytical Chemistry, 77(22), 7148–7155. https://doi.org/10.1021/ac050938g

Wang, L., Huang, D., Chan, C.K., Li, Y.J., Xu, X.G. (2017a) Nanoscale spectroscopic and mechanical characterization of individual aerosol particles using peak force infrared microscopy. Chemical Communications, 53(53), 7397–7400. https://doi.org/10.1039/c7cc02301d

Wang, X., Jing, B., Tan, F., Ma, J., Zhang, Y., Ge, M. (2017b) Hygroscopic behavior and chemical composition evolution of internally mixed aerosols composed of oxalic acid and ammonium sulfate. Atmospheric Chemistry and Physics, 17(20), 12797–12812. https://doi.org/10.5194/acp-17-12797-2017

Weingartner, E., Gysel, M., Baltensperger, U. (2002) Hygroscopicity of aerosol particles at low temperatures. 1. New low-temperature H-TDMA instrument: Setup and first applications. Environmental Science & Technology, 36(1), 55–62. https://doi.org/10.1021/es010054o

Wexler, A.S., Seinfeld, J.H. (1991) Second-generation inorganic aerosol model, Atmospheric Environment. Part A. General Topics, 25(12), 2731–2748. https://doi.org/10.1016/0960-1686(91)90203-J

Wexler, A.S., Clegg, S.L. (2002) Atmospheric aerosol models for systems including the ions H^+, NH_4^+, Na^+, SO_4^{2-}, NO_3^-, Cl^-, Br^-, and H_2O. Journal of Geophysical Research: Atmospheres, 107(D14), 4207. https://doi.org/10.1029/2001JD000451

Wills, J.B., Knox, K.J., Reid, J.P. (2009) Optical control and characterisation of aerosol. Chemical Physics Letters, 481(4–6), 153–165. https://doi.org/10.1016/j.cplett.2009.09.020

Wise, M.E., Biskos, G., Martin, S.T., Russell, L.M., Buseck, P.R. (2005) Phase transitions of single salt particles studied using a transmission electron microscope with an environmental cell. Aerosol Science and Technology, 39(9), 849–856. https://doi.org/10.1080/02786820500295263

Wise, M.E., Semeniuk, T.A., Bruintjes, R., Martin, S.T., Russell, L.M., Buseck, P.R. (2007) Hygroscopic behavior of NaCl-bearing natural aerosol particles using environmental transmission electron microscopy. Journal of Geophysical Research: Atmospheres, 112, D10224. https://doi.org/10.1029/2006jd007678

Wise, M.E., Freney, E.J., Tyree, C.A., Allen, J.O., Martin, S.T., Russell, L.M., Buseck, P.R. (2009) Hygroscopic behavior and liquid-layer composition of aerosol particles generated from natural and artificial seawater. Journal of Geophysical Research: Atmospheres, 114(D03201). https://doi.org/10.1029/2008JD010449

Wittmaack, K., Strigl, M. (2005) Novel approach to identifying supersaturated metastable ambient aerosol particles. Environmental Science & Technology, 39(21). 8177–8184. https://doi.org/10.1021/es0479538

Woods, E., Chung, D., Lanney, H.M., Ashwell, B.A. (2010) Surface morphology and phase transitions in mixed NaCl/$MgSO_4$ aerosol particles. The Journal of Physical Chemistry A, 114(8), 2837–2844. https://doi.org/10.1021/jp911133j

Woods, E., Yi, C., Gerson, J.R., Zaman, R.A. (2012) Uptake of Pyrene by NaCl, $NaNO_3$, and $MgCl_2$ Aerosol Particles. The Journal of Physical Chemistry A, 116(16), 4137–4143. https://doi.org/10.1021/jp3014145

Wu, H.B., Chan, M.N., Chan, C.K. (2007) FTIR Characterization of Polymorphic Transformation of Ammonium Nitrate. Aerosol Science and Technology, 41(6), 581–588. https://doi.org/10.1080/02786820701272038

Wu, L., Li, X., Ro, C.-U. (2019) Hygroscopic Behavior of Ammonium Sulfate, Ammonium Nitrate, and their Mixture Particles. Asian Journal of Atmospheric Environment, 13(3), 196–211. https://doi.org/10.5572/ajae.2019.13.3.196

Xi, J., Kim, J., Si, X.A., Zhou, Y. (2013) Hygroscopic aerosol deposition in the human upper respiratory tract under various thermo-humidity conditions. Journal of Environmental Science and Health, Part A>Toxic/Hazardous Substances and Environmental Engineering, 48(14), 1790–1805. https://doi.org/10.1080/10934529.2013.823333

Yeung, M.C., Lee, A.K.Y., Chan, C.K. (2009) Phase transition and hygroscopic properties of internally mixed ammonium sulfate and adipic acid (AS-AA) particles by optical microscopic imaging and Raman spectroscopy. Aerosol Science and Technology, 43(5), 387–399. https://doi.org/10.1080/02786820802672904

Yeung, M.C., Chan, C.K. (2010) Water content and phase transitions in particles of inorganic and organic species and their mixtures using Micro-Raman spectroscopy. Aerosol Science and Technology, 44(4), 269–280. https://doi.org/10.1080/02786820903583786

Yeung, M.C., Ling, T.Y., Chan, C.K. (2010) Effects of the polymorphic transformation of glutaric acid particles on their deliquescence and hygroscopic properties. The Journal of Physical Chemistry A, 114(2), 898–903. https://doi.org/10.1021/jp908250v

Zawadowicz, M.A., Proud, S.R., Seppalainen, S.S., Cziczo, D.J. (2015) Hygroscopic and phase separation properties of ammonium sulfate/organics/water ternary solutions. Atmospheric Chemistry and Physics, 15(15), 8975–8986. https://doi.org/10.5194/acp-15-8975-2015

Zelenay, V., Ammann, M., Křepelová, A., Birrer, M., Tzvetkov, G., Vernooij, M.G.C., Raabe, J., Huthwelker, T. (2011) Direct observation of water uptake and release in individual submicrometer sized ammonium sulfate and ammonium sulfate/adipic acid particles using X-ray microspectroscopy. Journal of Aerosol Science, 42(1), 38–51. https://doi.org/10.1016/j.jaerosci.2010.11.001

Zelenyuk, A., Imre, D., Han, J.-H., Oatis, S. (2008) Simultaneous measurements of individual ambient particle size, composition, effective density, and hygroscopicity. Analytical Chemistry, 80(5), 1401–1407. https://doi.org/10.1021/ac701723v

Zeng, G., Kelley, J., Kish, J.D., Liu, Y. (2014) Temperature-dependent deliquescent and efflorescent properties of methanesulfonate sodium studied by ATR-FTIR spectroscopy. The Journal of Physical Chemistry A, 118(3), 583–591. https://doi.org/10.1021/jp405896y

Zhang, Q.N., Zhang, Y., Cai, C., Guo, Y.C., Reid, J.P., Zhang, Y.H. (2014) In situ observation on the dynamic process of evaporation and crystallization of sodium nitrate droplets on a ZnSe substrate by FTIR-ATR. Journal of Physical Chemistry A, 118(15), 2728–2737. https://doi.org/10.1021/jp412073c

Zhang, Y.-H., Chan, C.K. (2000) Study of contact ion pairs of supersaturated magnesium sulfate solutions using Raman scattering of levitated single droplets. The Journal of Physical Chemistry A, 104(40), 9191–9196. https://doi.org/10.1021/jp0013659

Zhang, Y.-H., Chan, C.K. (2002) Understanding the hygroscopic properties of supersaturated droplets of metal and ammonium sulfate solutions using Raman spectroscopy. The Journal of Physical Chemistry A, 106(2), 285–292. https://doi.org/10.1021/jp012694j

Zhang, Y., Yuan, Q., Huang, D., Kong, S., Zhang, J., Wang, X., Lu, C., Shi, Z., Zhang, X., Sun, Y., Wang, Z., Shao, L., Zhu, J., Li, W. (2018) Direct Observations of Fine Primary Particles From Residential Coal Burning: Insights Into Their Morphology, Composition, and Hygroscopicity. Journal of Geophysical Research: Atmospheres, 123(22). https://doi.org/10.1029/2018jd028988

Zhao, L.-J., Zhang, Y.-H., Wei, Z.-F., Cheng, H., Li, X.-H. (2006) Magnesium sulfate aerosols studied by FTIR spectroscopy: hygroscopic properties, supersaturated structures, and implications for seawater aerosols. The Journal of Physical Chemistry A, 110(3), 951–958. https://doi.org/10.1021/jp055291i

Zuend, A., Marcolli, C., Booth, A., Lienhard, D.M., Soonsin, V., Krieger, U., Topping, D.O., McFiggans, G., Peter, T., Seinfeld, J.H. (2011) New and extended parameterization of the thermodynamic model AIOMFAC: calculation of activity coefficients for organic-inorganic mixtures containing carboxyl, hydroxyl, carbonyl, ether, ester, alkenyl, alkyl, and aromatic functional groups. Atmospheric Chemistry and Physics, 11(17), 9155–9206. https://doi.org/10.5194/acp-11-9155-2011

Zuend, A., Marcolli, C., Luo, B.P., Peter, T. (2012) A thermodynamic model of mixed organic-inorganic aerosols to predict activity coefficients. Atmospheric Chemistry and Physics, 12(21), 10075–10075. https://doi.org/10.5194/acp-12-10075-2012